RSC Advances

RSC Publishing

REVIEW

Recent advances in multifunctional magnetic nanoparticles and applications to biomedical diagnosis and treatment

Cite this: *RSC Advances*, 2013, **3**, 10598

Kai Yan,[a] Penghui Li,[b] Haie Zhu,[a] Yingjie Zhou,[a] Jingde Ding,[a] Jie Shen,[a] Zheng Li,[a] Zushun Xu*[ab] and Paul K. Chu*[b]

Received 23rd January 2013,
Accepted 21st March 2013

DOI: 10.1039/c3ra40348c

www.rsc.org/advances

By virtue of the unique magnetic properties and other functionalities, multifunctional magnetic nanoparticles (MNPs) are very promising in diagnostic and therapeutic applications. This review summarizes recent developments pertaining to the synthesis of MNPs with focus on the various surface modification strategies such as chemical synthesis, self-assembly, and ligand exchange. Recent applications of MNPs to multimodal imaging including magnetic resonance imaging (MRI)/optical imaging (fluorescent dyes, quantum dots (QDs), near-infrared absorption and up-conversion luminescence, MRI/positron emission tomography (PET), MRI/X-ray computed tomography (CT), and triple modality imaging are discussed. In addition, targeted drug and gene delivery, hyperthermia treatment for cancer, and other biomedical diagnosis rendered possible by MNPs are described.

1. Introduction

The integration of nanotechnology and molecular biology with chemistry, physics, engineering, materials science, and medical science spurs the development of the new field of nanobiotechnology and many novel nanobiomaterials with important applications to diagnosis and therapies have been designed and produced.[1–6] Among the various types of nanoparticles, magnetic nanoparticles (MNPs) such as Fe_3O_4 magnetite and γ-Fe_2O_3 maghemite are particularly appealing due to their super-paramagnetic properties, tunable size, and other biological functionalities.[7,8] Possessing a diameter smaller than the single domain limit, MNPs exhibit high saturation magnetization at room temperature in an external magnetic field but it disappears when the magnetic field is removed by thermal agitation. That is to say, magnetization of the MNPs can be altered with sufficient thermal energy.[9,10]

[a]*Ministry-of-Education Key Laboratory of Green Preparation and Application for Materials, Hubei University, Wuhan, 430062, P. R. China.*
E-mail: zushun25@yahoo.com.cn; paul.chu@cityu.edu.hk; Fax: 86-27-88665610; Fax: 852-34420542; Tel: 852-34427724 Tel: 86-27-88661879
[b]*Department of Physics & Materials Science, City University of Hong Kong, Tat Chee Avenue, Kowloon, Hong Kong, P. R. China*

Kai Yan

Mr Kai Yan joined Prof Xu's group at University of Hubei in 2011. His current scientific interests are devoted to fabricating the multifunctional magnetic nanoparticles, and their biomedical application, especially in multimodal imaging.

Penghui Li

Mr Penghui Li was born in 1986. He received a B.S. degree in polymer science and engineering from Hubei University, Wuhan, China, in 2008, where he received his M.S. degree in materials science in 2011. He is currently working toward his PhD degree in the Plasma Laboratory, Department of Physics and Materials Science, City University of Hong Kong, Kowloon, Hong Kong. His research interests include functional polymer microspheres, polymer films and coatings for surface modification of biomedical NiTi shape memory alloys.

Owing to these unique magnetic properties and a surface capable of being conjugated with many biological and drug molecules, MNPs have widespread applications in biological and medical science, for instance, in multimodal imaging,[11–13] targeted drug and gene delivery,[14,15] hyperthermia for cancer treatment,[16–18] biomedical separation,[19–22] tissue repair,[23,24] and catalysis.[25]

In practice, it is imperative to design materials with the proper size, shape, biocompatibility, surface functionality, and stability *in vitro* and *in vivo*. In general, MNPs are named according to their size. For instance, MNPs smaller than 40 nm are named ultra-small particles of iron oxide (USPIO) whereas those larger than 40 nm are named super-paramagnetic iron oxide (SPIO). A series of studies has confirmed the effects of size on hysteresis losses related to the magnetic field amplitude and reticuloendothelial system (RES) imaging behavior *in vivo*.[26,27] When they are injected into the body, SPIOs are taken up by macrophage and accumulate spontaneously in the liver or spleen. However, USPIO with a smaller size cannot accumulate in the RES system and exhibits a longer blood circulating time.[28] The body is rigidly regulated, particularly in terms of the blood flow, ionic strength, and physiological pH (7.35–7.45). Ideally, MNPs should be more soluble in an aqueous medium to improve *in vivo* transportation in biomedical applications. Furthermore, MNPs must be modified to improve the biocompatibility and prevent aggregation. Without surface modification, MNPs tend to aggregate into large clusters because of their large surface-to-volume ratio and dipole–dipole interaction. Several surface modification techniques have been developed using either organic materials (polymers such as dextran,[29,30] chitosan,[31] protein,[32,33] polyethylene glycol,[34–36] polyvinyl[37] and polyethylenimine[38]) or inorganic materials (Au,[39] Ag,[40] silica,[41] and carbon.[42]) In tumor detection, MNP carriers conjugated with target-specific biomolecules and possessing surface reactive moieties such as carboxylic groups, amine groups, and thiol groups should be able to travel in blood and recognize the desired targets *via* the specific biological interactions with nucleic acids, antibodies, peptides, and folic acid.

The objective of this review is to describe recent advances pertaining to the design, preparation, and application of magnetic nanoparticles for biomedical diagnosis and treatment. The review comprises three parts: common synthetic approaches to fabricating magnetic nanoparticles, different surface modification strategies, and biomedical applications such as multimodal imaging, targeted drug and gene delivery, and hyperthermia treatment of cancer.

2. Syntheses of magnetic nanoparticles

Magnetic nanoparticles have been prepared by physical methods such as mechanical grinding, gas phase deposition, electron beam lithography as well as chemical techniques such as co-precipitation, micro-emulsion synthesis, sol–gel synthesis, sonochemical synthesis, thermal decomposition, hydrothermal/solvothermal synthesis, and polyol synthesis. In comparison with physical synthesis, magnetic nanoparticles produced by wet chemical methods are better suited for biomedical applications because of the better control of the size, shape, and composition according to LaMer theory.[43] A suitable capping agent has to be used to prevent the magnetic nanoparticles from agglomerating. Some representative wet chemical synthesis routes and associated advantages and disadvantages are summarized in Table 1.[44,45]

2.1 Co-precipitation method

The synthetic methods for MNPs are divided into two main categories, hydrolytic and non-hydrolytic approaches. Co-precipitation of Fe^{2+} and Fe^{3+} salts in aqueous alkaline media (*e.g.* ammonia or sodium hydroxide solution) is the traditional hydrolytic means to generate iron oxides according to the Massart method.[46] In order to keep the average size of the MNPs between 4 and 20 nm, many experimental parameters including temperature, pH, nature of the base, and iron

Zushun Xu

Professor Zushun Xu, received his PhD in polymer science and engineering in 1998 from Zhejiang University, China. From Dec 1998 to Jun 2000, he worked as a Postdoctorate in South China University of Technology, China. From Jun 2000 to Jun 2002, he worked in Oklahoma State University, USA, as a Postdoctoral visiting scientist. His current research interests include the design and synthesis of multifunctional nanomaterials and biomedical applications.

Paul K. Chu

Professor Paul K Chu received his PhD in chemistry from Cornell University and is Chair Professor of Materials Engineering at City University of Hong Kong. He is fellow of the APS, AVS, IEEE, and MRS. His research activities focus on plasma surface modification as well as biomedical, microelectronic, and optoelectronic materials and devices. He has published more than 1,000 journal papers and given over 100 plenary, keynote, and invited talks at international conferences. He is ranked in the top 100 in materials science in the world by Thomson Reuters Essential Science Indicators.

Table 1 Comparison of common wet chemical techniques to synthesize magnetic nanoparticles

Synthetic method	Co-precipitation	Hydrothermal/solvothermal	Thermal decomposition
Precursor	Ferrous salt, ferric salt, for example	$FeCl_3 \cdot 6H_2O$, $FeSO_4 \cdot (NH)_4SO_4 \cdot 6H_2O$, for example	Iron acetylacetonate, iron carbonyl, cupferronates, for example
Reducing agent	Not necessary	Diethylene glycol, for example	Not necessary
Stabilizer	Necessary, *e.g.* sodium citrate	Necessary, *e.g.* polyacrylic acid	Necessary, *e.g.* oleic acid and oleylamine
Solvent	Water	Water/ethanol	Organic compound
Reaction step	Reaction at near room temperature followed by condensation	One step comprising liquid–solid–solid	Heating
Reaction T (°C)	20–90	180–220	100–300
Morphology	Spheres	Disks, spheres, needles	Spheres, cubes, triangles
Size (nm)	10–50	200–800	10–30
Magnetism (emu g^{-1})	30–50	50–90	60–120
Yield	Scalable	Medium	Scalable
Advantages	Cheap chemicals; mild reaction conditions	Tunable magnetism; tunable size; good crystallinity	Narrow size distribution; good control of the shape and crystallinity; tunable magnetism
Disadvantages	Poor control of size distribution; uncontrolled oxidation	High temperature; high pressure	Toxic organic compound; high temperature

concentration have been adopted to control the morphology, size, size distribution, and crystalline quantity. For example, Fe^{2+} and Fe^{3+} should have a 1 : 2 molar ratio in a non-oxidizing environment; otherwise the precipitate will be oxidized to the more stable γ-Fe_2O_3. According to thermodynamics, the pH should be between 9 and 14 as a high pH may induce repulsion producing smaller MNPs. Therefore, in order to improve the dispersibility and stability in the aqueous environment, the MNPs are often modified by diluted nitric acid, sodium citrate, sodium alginate, or other organic stabilizing agents like polyvinyl pyrrolidone.[47] Significant advance has been made in preparing monodispersed magnetite nanoparticles such as super-paramagnetic ferrite nanoparticles (MFe_2O_4, where M = Fe, Co, Mn) with high colloidal stability and enhanced saturation magnetization (up to 1.3 times) (Fig. 1a). They are synthesized by one-step aqueous co-precipitation using an alkaline agent such as alkanolamine, isopropanolamine, or diisopropanolamine, which acts as both the alkaline and complex agents to control the particle size during synthesis and improve the spin rearrangement on the surface.[48] At present, co-precipitation is still the preferred choice to produce water-dispersible MNPs in high yields because it offers many advantages such as mild reaction conditions, cost effectiveness, less time consuming, and easy scalability for industrial applications. However, it also suffers from the limitation that many experimental parameters must be controlled, thereby hampering many biomedical applications.

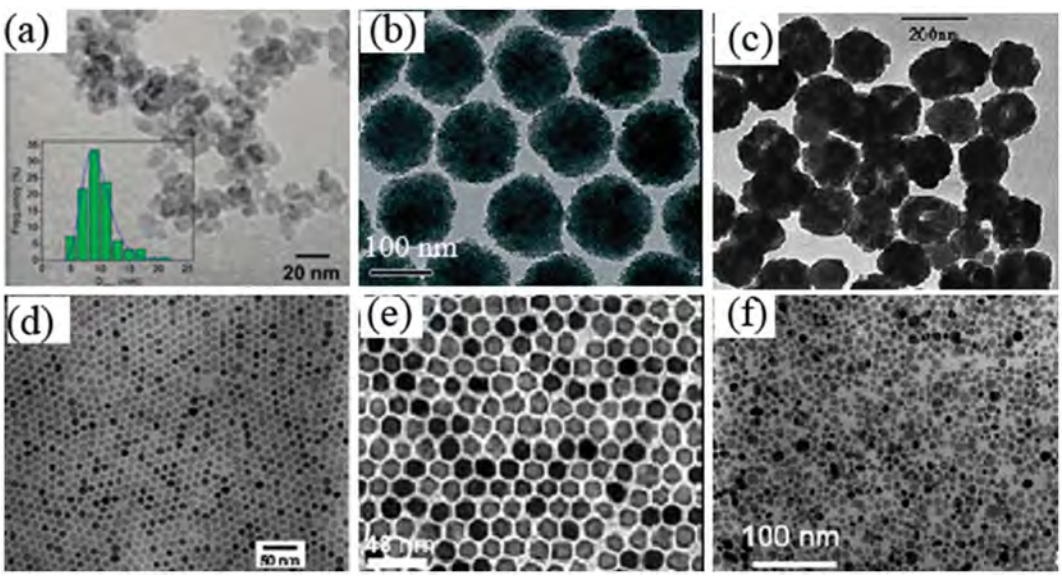

Fig. 1 TEM images of MNPs produced by different methods: (a) MNPs synthesized by co-precipitation using a new type of alkaline agent; (b) and (c) MNPs synthesized by the solvothermal/hydrothermal method; (d) and (e) MNPs synthesized by thermal decomposition; (f) MNPs synthesized by the one-pot reaction (images a, b, c, d, e and f are reprinted from ref. 48, 51–54, and 60 respectively, with permissions).

2.2 Hydrothermal/solvothermal method

In the mid-19th century, geologists began to study natural mineralization and hydrothermal/solvothermal methods. In these techniques, an aqueous solution is subjected to a high temperature and high pressure to dissolve substances with poor solubility under natural conditions. The reaction is conducted by controlling the temperature difference in the solution in the closed system to attain oversaturation resulting in precipitation and crystal growth.[49] This approach has become an important method to fabricate MNPs with improved magnetic properties. The mechanism of hydrothermal/solvothermal reactions and important conditions related to MNPs preparation have been discussed.[50] The organic solvent polyol is often used as the reaction medium in a sealed high-pressure reaction vessel (autoclave) at 80–200 °C for several days. During the reaction, the pressure is raised due to heating and enhances the solubility thus improve the crystallinity and reactivity of the nanoparticles produced. The typical synthesis of Fe_3O_4 and ferrite microspheres with a size range of 200–800 nm takes place in a solvothermal system *via* the modified reduction reactions between $FeCl_3$ and ethylene glycol. Ethylene glycol serves as a surfactant against particle agglomeration and sodium acetate as the electrostatic stabilizer to prevent particle agglomeration. Yin *et al.* have demonstrated the process for forming super-paramagnetic magnetite (Fe_3O_4) colloidal nanocrystal clusters (Fig. 1b), with each of which composed of many magnetite crystallites. The one step synthesis of the colloidal nanocrystal cluster building blocks incorporates the hydrolysis of $FeCl_3$ in a NaOH solution at a temperature above 220 °C in diethylene glycol and with polyacrylic acid (PAA) as the capping agent. The cluster building blocks were employed for constructing colloidal photonic crystals, and results showed that the unique optical response of these photonic crystals to external magnetic stimuli was rapid and fully reversible.[51] Li *et al.* have developed a facile one-pot, template-free method to prepare amine-functionalized magnetite nanoparticles and hollow nanospheres (Fig. 1c) with excellent magnetic properties. $FeCl_3{\cdot}6H_2O$ is the iron source and 1,6-hexadiamine serves as the ligand. The nanoparticles can be easily dispersed in water and conjugated to biological macromolecules such as peptides, proteins, and nucleic acids.[52] The main drawbacks of this method are the high processing temperature, hardware issues such as high pressure steel and corrosion-resistant lining, technical difficulty like precise control of temperature and pressure, long reaction time and relatively large MNP size. These negative factors can impact biomedical applications.

2.3 Thermal decomposition

Thermal decomposition based on pyrolysis of metal complexes precursors in the presence of a stabilizing ligand like oleic acid and oleylamine has recently become a common approach to produce high-quality nanoparticles with good crystallinity, morphology, and monodispersity as well as tunable size. The success of this method relies on the occurrence of a controlled burst of nucleation in the supersaturated solution, followed by crystal growth without additional nucleation according to the LaMer theory. It is achieved by controlling experimental parameters such as the reaction temperature, heating rate, and concentration of the metal complex and surfactant *via* hot injection or direct heating. The hot injection method is based on the formation of many nuclei when the metal complex is injected, whereas direct heating involves mixing of all the precursors and heating at a defined rate with the surfactants used to control the size and morphology. An organic solvent with a high boiling point is usually used as the reaction medium, whereas the metal complexes can be iron carbonyl $Fe(CO)_5$, $Fe(cup)_3$ (cup: N-nitrosophenylhydroxylamine, $C_6H_5N(NO)O$–), $Fe(acac)_3$ ($Fe(CH_3COCHCOCH_3)_3$), and iron oleate. For example, highly crystalline and monodispersed γ-Fe_2O_3 nanocrystallites have been produced by controlled oxidation of iron nanoparticles using trimethylamine oxide as the mild oxidant by the hot injection method. By controlling the experimental parameters, the particle size can be varied from 4 to 16 nm without further size selection[53] (Fig. 1e). Sun *et al.* have reported that in the presence of alcohol, oleic acid, and oleylamine, the high-temperature (265 °C) reaction of $Fe(acac)_3$ in phenyl ether can be carried out to produce size-controlled monodispersed Fe_3O_4 nanoparticles by direct heating (Fig. 1d). Using the smaller magnetite nanoparticles as seeds, larger monodispersed magnetic nanoparticles about 20 nm in size can be synthesized and dispersed into a nonpolar solvent.[54] By adopting a similar approach, the reaction between $Fe(acac)_3$, $Co(acac)_2$, or $Mn(acac)_2$ and the same diol produces monodispersed $CoFe_2O_4$ or $MnFe_2O_4$ nanoparticles with a tunable size between 3 and 20 nm by varying the reaction conditions or seed-mediated growth.[55] Kura *et al.* have prepared Fe nanoparticles in the range of 2.3 to 10 nm with high saturation magnetization (M_S) by thermal decomposition of the $Fe(CO)_x$–oleylamine ($x < 5$) reaction precursor. The ligands are different from conventional $Fe(CO)_5$ by partially replacing CO with oleylamine. The results confirm that the coordinate bond of the $Fe(CO)_x$–oleylamine exhibits a stronger coordinate tendency with Fe than CO and has significant influence on the size of the Fe nanoparticles.[56] Magnetic alloy nanoparticles (MANPs) such as FePt, $CoPt_3$, and FeCo which have higher magnetocrystalline anisotropy, larger coercivity, better chemical stability, and larger magnetic moments than ferrimagnetic nanoparticles are also used in the biomedical fields.[57] Monodispersed FePt MANPs are typically produced by thermal decomposition of iron pentacarbonyl, $Fe(CO)_5$ and reduction with platinum acetylacetonate, $Pt(acac)_2$, in the presence of 1,2-alkanediol. A small group of Fe and Pt atoms combine to form [FePt] clusters that act as the nuclei and the growth proceeds as more Fe–Pt species are deposited around the nuclei forming the MANPs. Based on the same mechanism, FeCo with controlled particle size has been synthesized by thermal decomposition of $Fe(acac)_3$ and $Co(acac)_3$.[58] According to the experimental results, the concentration and chemical nature of the precursors, the surface capping agent, the ratios of the precursors, and reaction temperature play important roles in the nucleation and growth of the nanoparticles

The monodispersed nanomaterials prepared by thermal decomposition and without undergoing surface modification are only soluble in nonpolar solvents, thereby limiting their use in biotechnology and biomedicine, especially *in vivo*

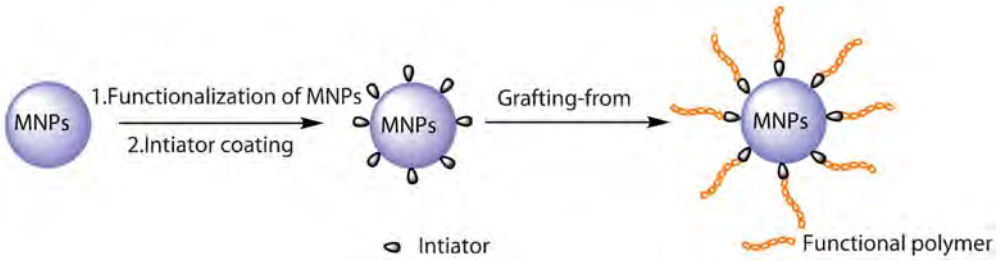

Fig. 2 Schematic diagram illustrating the surface-initiated living radical polymerization.

applications. Gao *et al.* have described a one-pot reaction to produce water-soluble iron oxide nanocrystals that inherit the advantages of thermal decomposition of $Fe(acac)_3$ in 2-pyrrolidone and surface coordination of the magnetic nanocrystals. The 2-pyrrolidone with strong polarity and a high boiling point not only serves as the medium in the high-temperature reaction, but also involves surface coordination which renders the magnetite nanocrystals with water-solubility and colloidal stability.[59] They have also synthesized biocompatible magnetic nanocrystals covalently covered by monocarboxy-terminated poly(ethylene glycol) (MPEG-COOH) by thermal decomposition of ferric triacetylacetonate in 2-pyrrolidone in the presence of MPEG-COOH (Fig. 1f). The carboxylate groups bind closely to the particle surface, and the preliminary MRI results indicate that the MNPs possess very good biocompatibility and a long blood circulation time.[60] There are other approaches to form water-soluble MNPs.[61] On the heels of rapid developments in the preparation of MNPs, many novel MNPs have been developed, for example, core/shell ($FePt/Fe_3O_4$,[62] Fe_3O_4/Au,[63]) spindle-like mesoporous (α-Fe_2O_3/ZnO,[64]) dumbbell (Au-Fe_3O_4,[65]) core/shell/shell (Fe_3O_4/Polypyrrole/Au,[66]) yolk-shell ($FePt@Fe_2O_3$,[67] $FePt@CoS_2$,[68]) ordered mesoporous ($Co_3O_4/CoFe_2O_4$,[69]) ordered mesoporous Fe_2O_3,[70] and so on.

3. Multifunctionalization of magnetic nanoparticles

3.1 Surface-initiated living radical polymerization (SILRP)

Attaching polymers or molecules onto nanoparticles surface by the ''grafting to'' or ''grafting from'' approaches is the key step to obtain hybrid core-shell nanoparticles with tailored properties. The ''grafting to'' strategy acquires MNPs coated with prefabricated polymers containing functional groups *via* either hydrophobic interactions or electrostatic attraction. However, this technique suffers from some limitations and often leads to low grafting density and small polymer thickness. Alternatively, the ''grafting from'' approach, mainly carried out in conjunction with surface-initiated living radical polymerization (SILRP), can produce a high grafting density and better stability of the polymer shell. SILRP illustrated in Fig. 2 starts with the formation of active sites on the particle surface to become the ''living'' radical for polymerization. In the presence of a monomer, the radical propagates until it is deactivated back to the polymer chain. In the frequent activation–deactivation cycles, each ''living'' chain has a nearly equal chance to grow, consequently yielding polymer chains with low dispersity.[71] The molecular weight, polydispersity, and density of the polymer chains ''grafted'' from the surface can be easily controlled.[72] Typical SILRP processes are based on the following different mechanisms: atom transfer radical polymerization (ATRP), reversible addition-fragmentation chain transfer (RAFT), nitroxide-mediated radical polymerization (NMRP), and ring-opening polymerization (ROP).

ATRP is a versatile and robust technique first reported in 1995.[73] It has been most extensively utilized to produce hybrid core-shell nanoparticle brushes. In this technique, polymer chains can propagate from the nanoparticle surface, and end-functionalized or block copolymerized polymers provide a variety of active sites for further multi-biofunctionalization.[74] ATRP is conducted on magnetic surfaces by two different routes, physical absorption of acid-containing halides and covalent bonding of ATRP initiating halides *via* silanation. For instance, 3-chloropropionic acid (CPA) can initiate the formation of poly(ethylene glycol) methacrylate (PEGMA) to produce monodispersed PEGMA-grafted magnetic nanoparticles. Monodispersed MNPs with fluorescent characteristics can be obtained by using 3-aminopropyltrimethoxysilane as the anchor molecules in post polymerization modification, followed by chemical attachment of fluorescein isothiocyanate (FITC) to the amine groups.[75] The MNPs are coated by poly(glycidyl methacrylate-*co*-poly(ethylene glycol) methyl ether methacrylate) by ATRP using the reaction product of γ-aminopropyl triethoxysilane and 2-bromoisobutyryl bromide as the initiator. PEGMA in the copolymer chains endows the nanoparticles in an aqueous medium with high stability and prevents recognition by macrophages with the aim of prolonging their circulation time *in vivo*. Glycidyl methacrylate (GMA) groups have been used to conjugate folic acid (FA) to target cancer cells *via* 'click' chemistry.[76] Majewski *et al.* have developed the macro-initiator with the surface-functionalized dopamine anchor group *via* ligand exchange. In this process, 2-(dimethylamino) ethyl methacrylate (DMAEMA) is polymerized on the surface by ATRP to produce dual-responsive (pH and temperature) core-shell magnetic composites (γ-Fe_2O_3@PDMAEMA). The hybrids have high stability in aqueous media for over six months and are suitable as a transfection reagent in biotechnological applications because of the ability to form polyelectrolyte complexes with DNA.[77] In the normal ATRP system, the catalyst complex contains a transition-metal compound that is sensitive to oxygen and can

easily be oxidized to a higher oxidation state, and hence, polymerization can be easily influenced by oxygen. To overcome these drawbacks, electron transfer ATRP employing a reducing agent is conducted in air. The initiator for ATRP is modified on magnetic nanoparticles *via* ligand exchange with 3-aminopropyltriethoxysilane (APTES) and then esterification with 2-bromoisobutyryl bromide. The fluorescent monomer 9-(4-vinylbenzyl)-9*H*-carbazole (VBK) and hydrophilic monomer PEGMA are grafted from the magnetic nanoparticles (ferroferric oxide) *via* electron transfer ATRP using $FeCl_3 \cdot 6H_2O$ as the catalyst, tris(3,6-dioxaheptyl)amine as the ligand, and ascorbic acid as the reducing agent to produce magnetic and fluorescent nanoparticles[78] (Fig. 3).

Compared to ATRP with metal agents, RAFT works with more vinyl monomers without metal catalysts under milder conditions. However, it may be difficult to covalently attach RAFT agents to magnetic nanoparticles. For example, the *S*-1-dodecyl-*S*′-(α, α-dimethyl-α′′-acetic acid) trithiocarbonate chain transfer agent (CTA) is immobilized on Fe_3O_4 nanoparticles to obtain Fe_3O_4@CTA and then the thermoresponsive polymer poly (*N*-isopropylacrylamide) (PNIPAM) chains are grafted from the surface of Fe_3O_4@CTA *via* surface initiated reversible addition-fragmentation transfer (RAFT) polymerization.[79] Moreover, trichloro(4-chloromethylphenyl) silane can be immobilized on the surface of magnetic silica hybrid MNPs prepared by the modified Stöber method to form chloromethylphenyl functionalized silica Fe_3O_4@SiO_2-Cl, followed by the reaction with carbazole, KOH and CS_2 to synthesize the fluorescent RAFT agent. Eventually, water soluble trifunctional MNPs with thermoresponsive, magnetic and fluorescent properties are produced by surface initiated RAFT polymerization using NIPAM as the monomer.[80] Takahara *et al.* have proposed the chemisorbed initiator with a NMRP moiety that contains 2,2,6,6-tetramethylpiperidinyl-1-oxyl (TEMPO) in nitroxide-mediated radical polymerization and a phosphoric acid moiety that can interact with the magneteta-OH groups to produce controlled polystyrene and poly(3-vinylpyridine) graft layers on the surface of magnetic nanoparticles. In this way, polymer-grafted magnetite (Fe_3O_4) nanoparticles with a diameter of about 10 nm can be produced.[81]

ATRP requires the use of a metal catalyst and a ligand with low toxicity. They may contaminate the final product and cause problems in biomedical applications. RAFT also faces the same problem associated with biological toxicity due to the disulfide bonds of the RAFT reagents. Although NMRP does not require a catalyst, it is subjected to certain restrictions concerning the kind of reactive monomers.

3.2 Self-assembly

Magnetic nanoparticles produced by pyrolysis (or thermal decomposition) are usually hydrophobic and not suitable for biological applications. To overcome the obstacle, there are different ways to disperse the hydrophobic MNPs in aqueous solutions. Polymeric micelles have drawn considerable interest because of potential applications to anticancer drug delivery and diagnostic imaging.[82] Polymeric micelles are formed by the self-assembly of amphiphilic block copolymers with distinct hydrophobic and hydrophilic segments such as amphiphilic poly(3-caprolactone)-*b*-poly(acrylic acid) (PCL-PAA),[83] methoxy poly(ethylene glycol)-poly(*b*-amino ester)-sulforhodamine (PEG-PAE-S) block copolymer,[84] and other block copolymers. They possess the unique core-shell architecture (usually 10 to 100 nm) in an aqueous medium. The hydrophobic segments can interact with the oily surface of the MNPs and also serve as a natural carrier to load hydrophobic drugs or other imaging agents. The hydrophilic shells such as amino, carboxyl, and hydroxyl groups allow the particles to stabilize in the aqueous solution and steric repulsion hampers

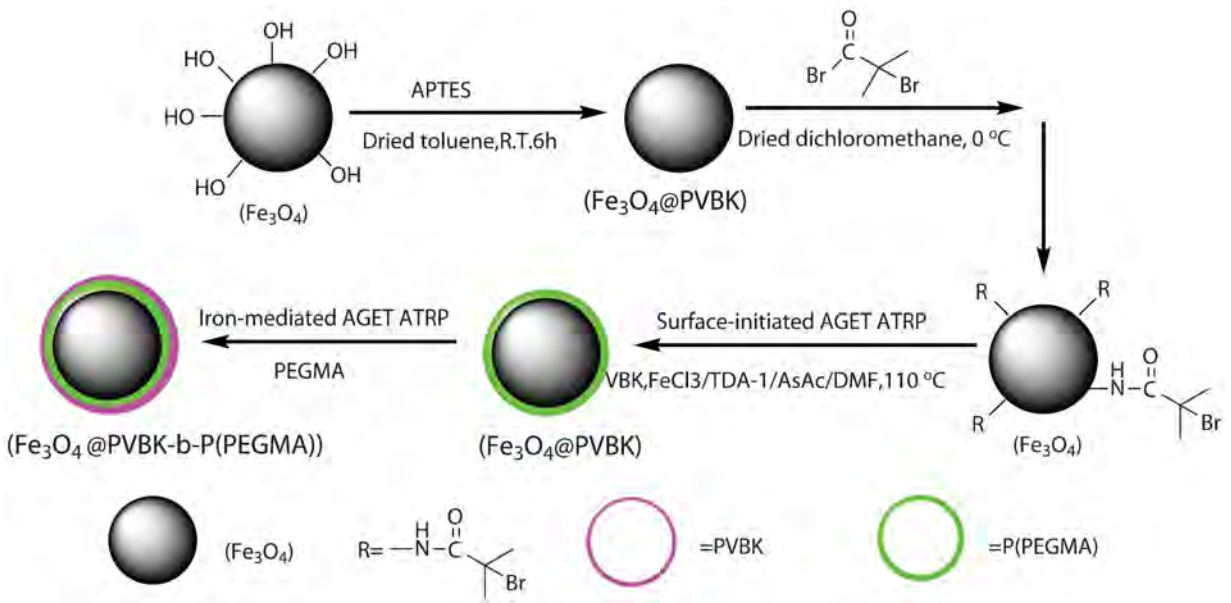

Fig. 3 Schematic diagram illustrating the preparation of polymer-grafted MNPs (Fe_3O_4@PVBK-*b*-P (PEGMA)) with the core/shell structure (reprinted from ref. 78 with permission).

MNPs aggregation. The amphiphilic diblock copolymer poly (ε-caprolactone)-poly(ethylene glycol)(PCL-PEG) synthesized by ring-opening polymerization of ε-caprolactone using monomethoxy-terminated PEG as the macro-initiator can produce the polymeric micelles. The PCL segment forms the hydrophobic core and hydrophilic PEG provides the protective shell. A cluster consisting of organic magnetite particles is encapsulated resulting in considerable increase in the MRI relaxivity. After attaching the molecular targeting ligand folate on the micelle surface, the multifunctional targeting system can transport anticancer drugs encapsulated inside the cores to tumor cells effectively.[85]

Taton *et al.* have demonstrated that amphiphilic poly(styrene$_{250}$-*block*-acrylic acid$_{13}$) (PS$_{250}$-*b*-PAA$_{13}$) co-assembles with magnetic nanoparticles to enclose the particles within the copolymer micelles (Fig. 4a).[86] Park *et al.* have shown that the incorporation drastically affects the self-assembled structure of the amphiphilic block copolymer (PAA-*b*-PS) by modifying the relative volume ratio between the hydrophobic and hydrophilic blocks. Three distinct assembly structures are obtained by controlling the interactions between the solvent and polymer nanoparticles: (a) polymer micelles in which nanoparticles are homogeneously incorporated (magneto-micelles), (b) core-shell type polymer assemblies in which nanoparticles are radially arranged at the interface between the polymer core and shell (magneto-core shell), and (c) polymersomes densely packed with nanoparticles (magneto-polymersomes). Among the three assemblies, magneto-polymersomes show higher relaxivity rates because of the larger number of nanoparticles pre-assembled and better water accessibility. More importantly, it enables the preparation of nanoparticle-encapsulating amphiphilic block-copolymer assemblies.[87] Fluorescent surfactants such as amphiphilic pyrenyl polyethylene glycol (Py-PEG) are synthesized by conjugation of hydrophilic PEG (polyethylene glycol) with hydrophobic and fluorescent 1-pyrenebutyric acid *via* esterification, and then $MnFe_2O_4$ nanocrystals are encapsulated to produce fluorescent magnetic composites with good water solubility. *In vitro* and *in vivo* studies have shown that the biocompatible fluorescent magnetic composites exhibit not only excellent sensitivity and feasibility as MRI probes but also high illumination intensity and strong signal strength in spite of short exposure time as UV imaging probes.[88] We have produced stable magneto-micelles by self-assembly of fluorine-containing amphiphilic (2,2,3,4,4,4-hexafluorobutyl methacrylate-*g*-methoxy poly(ethylene glycol) monomethacrylate) poly(HFMA-*g*-PEGMA) copolymers with oleic acid modified Fe_3O_4 nanoparticles in an aqueous medium (Fig. 4b). The fluorocarbon segments form a stable hydrophobic core to adsorb oil-based nanoparticles and the PEGMA segments enhance the solubility in water thus reducing the cytotoxicity of the hybrid micelles. Controlled release of hydrophobic drug 5-fluorouracil is achieved from the magneto-micelles with a loading efficiency of 20.94 wt%. The transverse relaxivity rate is 134.27 mM^{-1} s^{-1} and a high efficacy as a negative MRI agent in T_2-weighted imaging is demonstrated. Our results suggest that these magneto-micelles are potential nanocarriers in drug delivery and MRI contrast agents *in vivo*.[89]

Unlike amphiphilic block copolymers which are not soluble in water as unimers, polyelectrolyte-neutral block copolymers can spontaneously self-assemble to form the electrostatic complexes with a core-shell microstructure in the presence of charged aqueous species. For example, Held *et al.* have demonstrated that crystalline and monodispersed maghemite (Fe_2O_3) nanoparticles can be effectively transferred into an aqueous medium with no loss of structural and magnetic properties using the positively-charged tetramethylammonium hydroxide stabilized at neutral pH by means of ligand exchange. When the block copolypeptide poly (N_e-2[2-(2-methoxyethoxy)ethoxy]acetyl-L-lysine)$_{100}$-*b*-poly(L-aspartic acid, sodium salt)$_{30}$ (poly(EG$_2$-lys)$_{100}$-*b*-poly-(asp)$_{30}$) is introduced into an aqueous dispersion of maghemite nanoparticles, the nanoparticles cooperatively assemble into clusters because of favorable electrostatic interactions between the aspartic acid residues and nanoparticles.[90] Based on electrostatic complexing, Berret *et al.* have reported the formation of new hybrid aggregates consisting of super-paramagnetic nanoparticles (maghemite γ-Fe_2O_3) and cationic-neutral copolymers poly (trimethylammonium ethylacrylate methyl sulfate)-*b*-poly-(acrylamide) (PTEA-*b*-PAM) based on electrostatic adsorption and charge compensation between oppositely charged species.[91] The magnetic clusters are larger with PTEA (11 K)-*b*-PAM (30 K) than with PTEA (5 K)-*b*-PAM (30 K), suggesting that the molecular weight of the polyelectrolyte blocks is an important parameter in controlling the size of the hybrids.

As a facile and practical method to prepare polyelectrolyte capsules in biomedical applications, layer-by-layer self-assembly in which the multilayers are formed based on alternating electrostatic adsorption of molecular layers with oppositely charged polymers has attracted much attention. The technique has several advantages such as wide and simple selection of materials for assembly and ability to fine tune the self-assembly architecture with controlled permeability. Li *et al.* have synthesized cationic and anionic curcumin (Cur) conjugates by anchoring Cur onto poly-(vinylpyrroidone) (PVP-Cur) and hyaluronic acid (HA-Cur) to modify positively-charged amino-terminated magnetic nanoparticles (*N*-3-trimethoxy silyl propyl ethylene diamine@MNPs) and to construct six double layers of curcumin conjugates by layer-by-layer assembly. The HA is coated onto the outer surface to form HA (HA-Cur/PVP-Cur)$_6$@MNPs (Fig. 4d) which exhibit more cytotoxicity than free curcumin. This is attributed to the enhanced solubility along with better absorption *via* hyaluronic acid receptor-mediated endocytosis.[92] Cho *et al.* have demonstrated successful preparation of multifunctional silica colloids coated with poly-(amidoamine)/2-bromo-2-methylpropionic acid-stabilized iron oxide particles (PAMA/BMPA-Fe_3O_4)$_n$ or/and BMPA-stabilized quantum dots (PAMA/BMPA-CdSe@ZnS)$_n$ multilayers[93] using layer-by-layer assembly based on a nucleophilic substitution reaction between the bromo and amine groups in organic media. These colloids possess strong magnetic and photoluminescent properties with reversible optical tuning under an external magnetic field. The highly protuberant and rugged surface morphology of multifunctional silica colloids gives rise to surface super-hydrophobicity manifested by a water contact angle exceeding 150°.

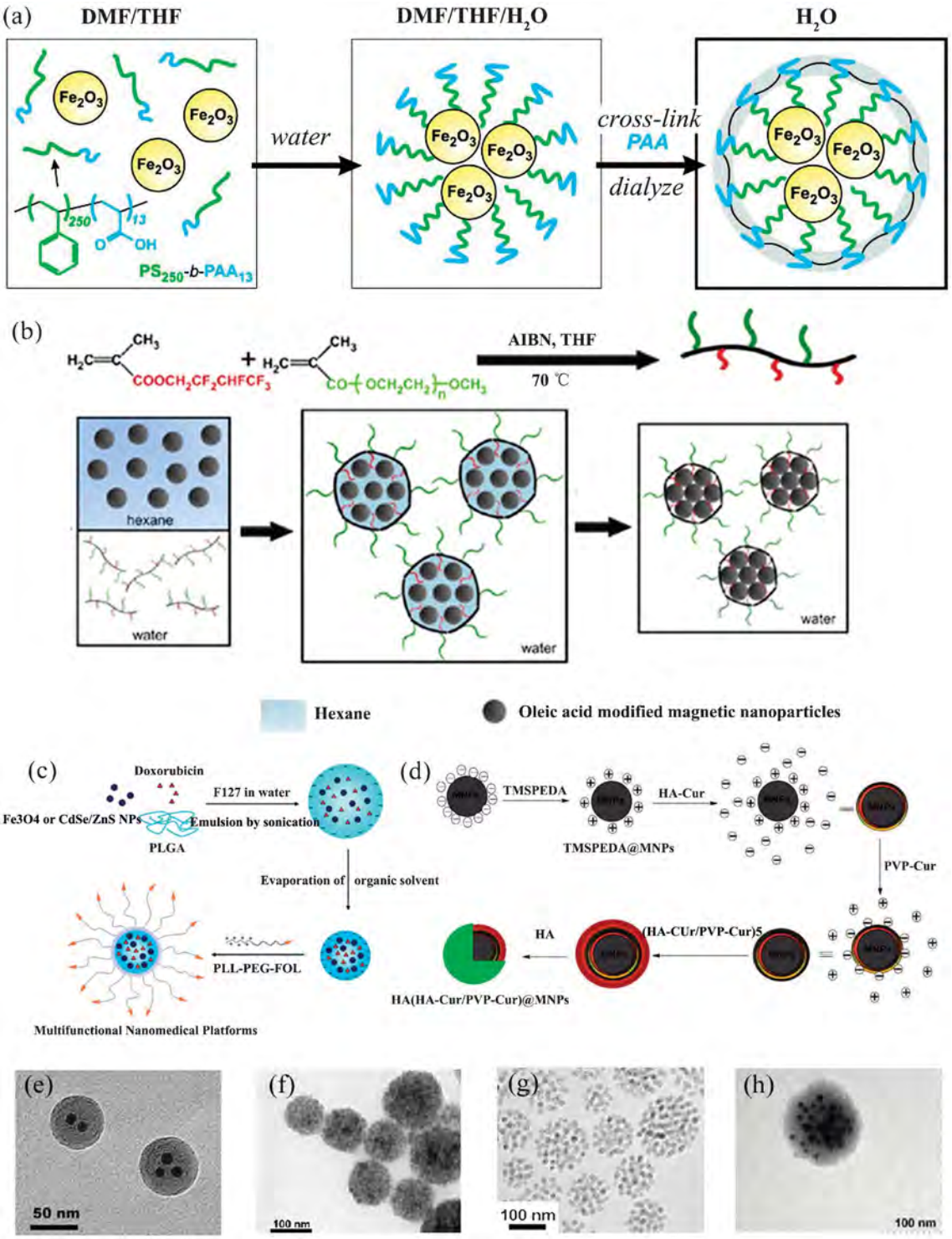

Fig. 4 Schematic illustration of the formation of magneto-micelles during self-assembly and TEM images: (a) MNPs@PS_{250}-*b*-PAA_{13}, corresponding to TEM (e); (b) MNPs@HFMA-*g*-PEGMA corresponding to TEM (f); (c) PLGA (MNPs/DOXO)-FOL corresponding to TEM (g); (d) $(HA\text{-}Cur/PVP\text{-}Cur)_6$@MNPs corresponding to TEM (h) (images a and e, b and f, c and g, d and h are reprinted from ref. 86, 89, 92, 94, respectively, with permissions).

The solvent evaporation/extraction technique has been utilized to prepare magneto-micelles. In brief, MNPs and doxorubicin (DOX) are put into biodegradable poly(D,L-lactic-*co*-glycolic acid) (PLGA) which is then incorporated into the hydrophobic part of the $F_{127}((EO)_{97}(PO)_{69}(EO)_{97})$ micelles upon evaporation of the organic solvent. Afterwards, the folate is conjugated onto the PLGA nanoparticles by polyethylene glycol PEG groups to target KB cells. The multifunctional polymer

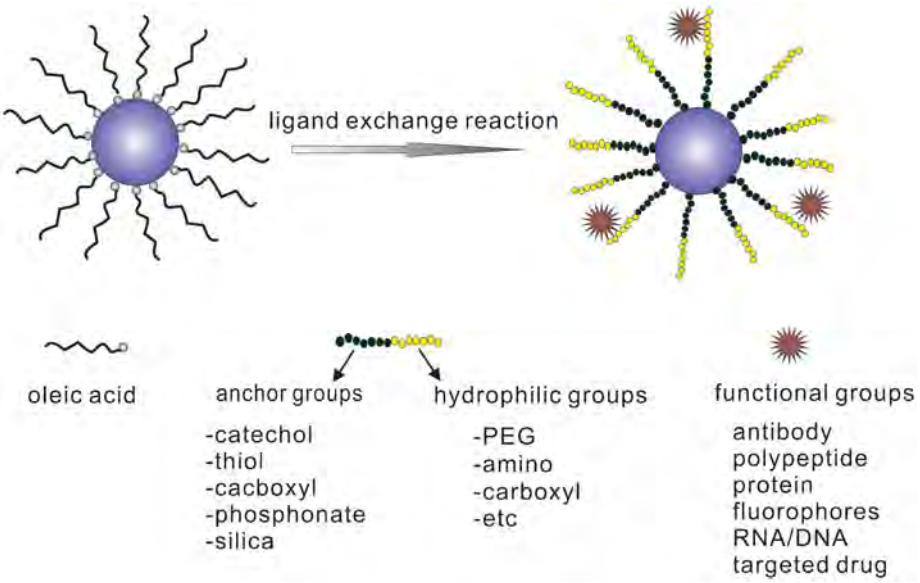

Fig. 5 Schematic diagram illustrating the typical process in the ligand exchange reaction.

nanomedical platform has been developed to provide effective targeting to folate receptors, detection by MRI, optical imaging, and cell growth inhibition in KB cancer cells (Fig. 4c).[94] Similarly, Fe_3O_4 can be encapsulated inside poly (L-lactic acid)-*block*-poly (poly (ethylene glycol) monomethacrylate) (PLLA-*b*-PPEGMA). The block copolymer is prepared by ring-opening polymerization of lactide with a double-headed initiator, 2-hydroxyethyl 20-methyl-20-bromopropionate (HMBP) and then atom transfer radical polymerization (ATRP) of PEGMA using a solvent evaporation/extraction technique. After further functionalization with folic acid, the magneto-micelles exhibit great efficacy in targeting MCF-7 cancer cells.[95]

3.3 Ligand exchange

Encapsulation of multiple iron oxide cores in one cluster by macromolecular dispersants leads to a hydrodynamic diameter many times larger than the core diameter and a broad size distribution. It poses problems for biomedical applications in living organisms, especially concerning cardiovascular magnet resonance imaging (MRI) and MRI of extravascular targets which requires ultra small particles. Although thermal decomposition produces monodispersed particles, the drawback is that the resulting nanoparticles are only soluble in nonpolar solvents. Consequently, efforts have been made to focus on the chemical side such as ligand exchange to modify the surface properties of nanoparticles. In this technique, excess ligands are added to the solution to displace the original ligands on the surface of the nanoparticles (Fig. 5). According to Pearson's theory of hard and soft acids and bases (HSAB),[96] the anchoring groups have strong binding ability to MNPs and can provide much better colloidal ability under physiological conditions than other approaches. The ligands can be classified as multifunctional molecular ligands and multidentate polymeric ligands. Most of them have powerful anchoring components such as carboxylic, phosphate, sulfate, thiol, and catechol groups. Inspired by the thiol ligand exchange on gold and platinum nanoparticles, Hong has developed a strategy to cover FePt nanoparticles with PEGylate thiol and dopamine which are essential to water solubility and stability *via* ligand exchange. Studies on mercaptoalkanoic acid ligand-exchanged FePt suggest binding of the carboxylate end to iron atoms and the mercapto end to platinum atoms. The surface thiol ligands can be exchanged with positively and negatively charged ligands and the magnetic nanoparticles surface can bind to biomolecules such as both DNA and proteins.[97] Huh has introduced a simple and high effective 2,3-dimercaptosuccinic acid (DMSA) ligand onto the nanocrystal surface by mixing the nanocrystals with a large excess of DMSA. This ligand binds to the iron oxide nanocrystal surface by carboxylic bonding and the intermolecular disulfide cross-linking between the surface-bound DMSA ligands strengthens the nanocrystal stability. The resulting DMSA-coated Fe_3O_4 nanocrystals with a size of 9 nm are fairly stable in water and phosphate-buffered saline (PBS) without showing aggregation.[98] The remaining free carboxylic acid and thiol groups render the nanocrystals hydrophilic and can be used to conjugate with targeting antibody Herceptin which has specific binding ability against a HER2/neu receptor over-expressed in breast cancer cells. Subsequent utilization of these conjugates as MRI probes for the monitoring of selective targeting events of human cancer cells implanted in live mice has been successfully demonstrated *in vivo*.[99]

A dendron-based surface-functionalization approach increases slightly the hydrodynamic diameter compared to the inorganic core and it is of specific interest to cardiovascular MRI and MRI of extravascular targets. Kim *et al.* have introduced hydroxamic acid based dendron linkers to exchange stearic acid from iron oxide to form a five-member chelating ring instead of a four-member ring or monodendate binding.[100] Hofmann have compared different bulky multi-

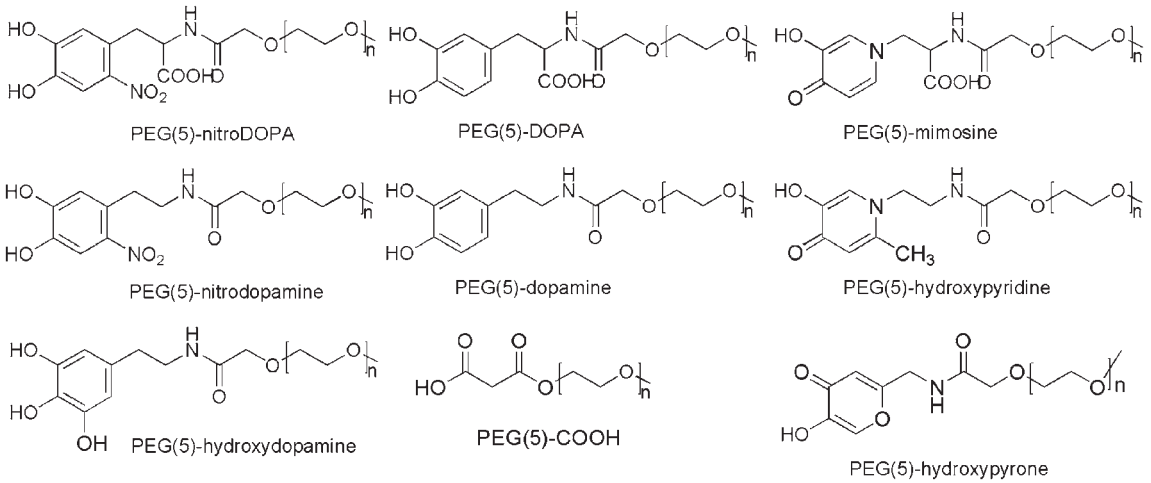

Fig. 6 Stabilization of iron oxide nanoparticles by using different functional ligands (reprinted from ref. 105, with permission).

functionalized hydroxamic acids containing dendron ligands with simple one-chain carboxylic acids containing hydroxamic acids with respect of their ligand exchange behavior with iron oxide nanoparticles. The stability of the nanoparticles in physiological media and the cytotoxicity of these systems are compared as well. The bulky dendron ligands with a small number of polar carboxylic acid groups are best suited for stabilizing the nanocrystals in polar solvents.[101] Huang has demonstrated that the peptide, synthesized with a poly(ethylene glycol) (PEG) linker followed by a cysteine residue at the C-terminus of the peptide (NH_2-RGDLATLRQL-PEG11-Cys-COOH or LCPPEG-Cys) can replace the hydrophobic surfactants on the as-synthesized magnetic nanoparticles, due to the bi-dentate binding to the Fe ions from the thiol and carboxylate groups on Cys. The MNPs exhibit specific targeting to the avb6-postive H2009 cells over avb6-negative H460 cells by controlling the T_2-weighted MR imaging.[102]

Among the various arching groups, catechol is one of the most highly regarded because of its strong binding force. In an effort to elucidate the coordination mechanism about dopamine with magnetic nanoparticles, Xu has employed dopamine as a robust anchor to immobilize the functional molecules on the shells of magnetic nanoparticles and used nitrilotriacetic acid (NTA) as the functional molecule for protein separation.[103] Reimhult *et al.* have shown that the layer-by-layer technique can build up successive shells of super-paramagnetic iron oxide nanoparticles individually stabilized with the high binding affinity of mPEG(550)-gallol and biotin-PEG(3400)-gallol. Furthermore, they are functionalized with biotinylated human anti-VCAM-1 antibodies using the biotin-neutravidin linkage, suggesting suitability for *in vivo* imaging of atherosclerosis.[104] Reimhult *et al.* have investigated the design principles for optimized anchors for dispersants to stabilize iron oxide nanoparticles using eight different catechol derivatives and PEG(5)-COOH (Fig. 6). Differential scanning calorimeter (DSC), dynamic light scattering (DLS), thermogravimetric analysis (TGA), and X-ray photoelectron spectroscopy (XPS) suggest that nitroDOPA and nitrodopamine are superior in providing a high dispersant of the nanoparticles and the particles stability is strongly correlated with the high dispersant packing density.[105]

Recently, Lee has developed an antibiofouling copolymeric system comprising a ''surface anchoring moiety'' (silane group) and ''protein-resistant moiety'' (PEG). By using a PEG-silane copolymer system, protein- and cell-resistant surfaces can be generated on Si/SiO_2 substrates by forming polymeric monolayers (PMs) *via* multiple covalent bonds. An antifouling 3-(trimethoxysilyl)propyl methacrylate-*r*-poly(ethylene glycol) methyl ether methacrylate (poly(TMSMA-*r*-PEGMA)@SPION) has been produced to detect tumors *in vivo* using clinical MRI. It is potentially efficient as a cancer diagnostic probe.[106] Larsen *et al.* have magnetically separated nanoparticles with biocompatible silane-PEG into two distinct size subpopulations with mean diameters of 20 and 40 nm. They exhibit different accumulation into macrophages *in vitro* and murine tumors after intravenous injection. The enhanced MRI contrast of the larger MNPs in the tumor can be accounted for the combined result of the size dependent extravasation and capture by macrophages in the tumor, thus providing important consideration to improved bioimaging.[107] Palma *et al.* have used silane with different end groups and alkane chain lengths to perform ligand exchange. The characteristics of the silane layer deposited on the particle surface depend on reaction variables such as the type of solvent, reaction time, catalyst, anchor group, and silane concentration. Amino-, carboxylic acid- and poly(ethylene glycol)-terminated silanes are found to render the MNPs with highly stability and water-dispersion because of the electrostatic and/or steric repulsion.[108] Pothayee *et al.* have reported the fabrication of magnetic block ionomer complexes based on the assembly of poly (ethylene oxide-*b*-acrylate) (PEO-*b*-PAA) ionomers with nanomagnetite and gentamicin. The (PEO-*b*-PAA) is bound to the magnetic nanoparticle surfaces by ligand adsorption of the PAA block, thereby creating a double corona structure. The nonionic PEO shell serves as a block copolymer segment to improve biocompatibility and the ionic region rich in PAA can be utilized to bind with high concentrations of gentamicin with multiple cationic sites.[109]

Table 2 Size and size distribution of microspheres in different polymerization methods[110]

Polymerization technique	Diameter (μm)	Size distribution
Microemulsion	0.008–0.08	Narrow
Emulsion	0.1–0.15	Narrow
Soap-free emulsion	0.1–0.5	Narrow
Miniemulsion emulsion	0.05–0.1	Relatively narrow
Dispersion	5–20	Narrow
Seed emulsion	1–2	Narrow
Precipitation	10	Narrow
Suspension	100	Wide

3.4 Various heterogeneous polymerization techniques

Various heterogeneous polymerization techniques have been used to synthesize magnetic nanocomposites with different sizes and size distributions for biomedical applications and examples include suspension polymerization, dispersion polymerization, microemulsion polymerization, mini(emulsion) polymerization, inverse emulsion polymerization, and soap-free emulsion polymerization. The key of these polymerization techniques lies in the preliminary modification of the magnetic nanoparticles, choice of monomer with hydrophilic and hydrophobic property, as well as the appropriate surfactant. Some typical polymerization techniques for nanocomposites are summarized in Table 2.

Emulsion polymerization is one of the common methods to synthesize functional nanocomposites with different structures. For example, sub-micrometer-sized citrate-acid stabilized Fe_3O_4 nanoparticles can be modified by 3-(trimethoxysilyl)propyl methacrylate (MPS) to immobilize the active vinyl groups on the surface and the hydrophobic monomers styrene is polymerized at the interface to form the polymer shells *via* seeded emulsion radical polymerization. The morphology of the composite microspheres can be made into raspberry- and flower-like (Fig. 7e) or eccentric structures by adjusting the weight ratio of the seed to the monomer (Fe_3O_4/St) and varying the amount of cross-linker divinyl benzene (DVB).[111] Fe_3O_4 colloidal nanocrystal clusters can be further functionalized with a monolayer of coupling agent [3-(methacryloyloxy) propyl] trimethoxysilane (MPS) through siloxane linkage, and monodispersed Fe_3O_4@SiO_2@PS core-shell spherical colloids can be produced by one-step emulsion polymerization of styrene using MPS grafted Fe_3O_4@SiO_2 as the seed and sodium dodecyl sulfate as a surfactant[112] (Fig. 7f). Hydrogels are widely used because of desirable features such as their hydrophobic group and hydrophilic residue, water solubility, and soft crosslinked network. In biological applications of MNPs, magnetic hydrogels with supra-colloidal structures are fabricated by suspension polymerization. It is based on Pickering emulsion droplets of *N*-isopropylacrylamide (NIPAm) and acrylamide (Am) with different NIPAm/Am ratios and the Fe_2O_3 nanoparticles are stabilized in the droplets.[113] The main feature of this approach is that MNPs can self-assemble at the liquid–liquid interfaces to form stable water in oil Pickering emulsion droplets. This leads to other methods to synthesize a variety of hybrid hydrogels with supra-colloidal structures.

Microemulsion is a powerful tool to prepare MNPs with controlled size. Microemulsions are thermodynamically stable colloidal dispersions because of the presence of a monolayer of surfactant. Okoli *et al.* have successfully prepared MNPs from water-in-oil (w/o) and oil-in-water (o/w) micro-emulsions using a cationic surfactant and nonionic surfactant, respectively and investigated the binding and separation capacity of MNPs with proteins.[114] One of the disadvantages of this technique is that the purification step of the product is cumbersome and so soap-free emulsion polymerization has invoked interest in biomedical applications because this method can produce monodispersed and ''clean'' particles with low cytotoxicity without the use of surfactants. For instance, Mikio Konno has synthesized highly monodispersed particles composed of magnetic silica core and fluorescent

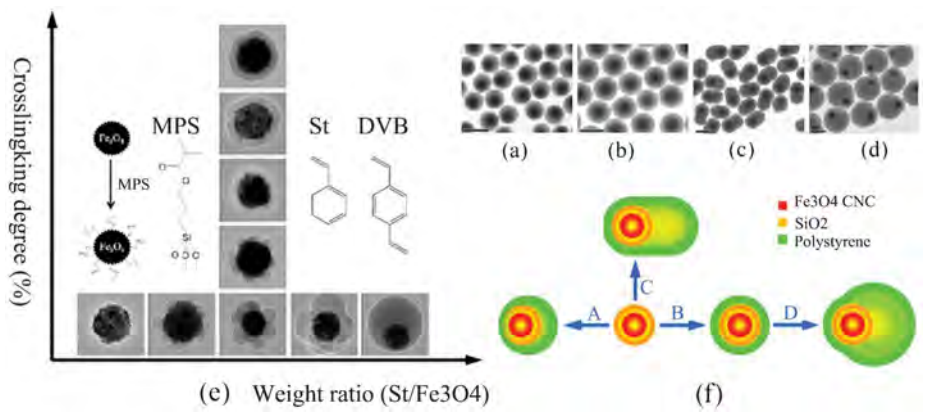

Fig. 7 TEM images of a series of Fe_3O_4@SiO_2@PS composite colloids with complex structures/shapes: (a, b) Spherical colloids produced in one-step emulsion polymerization (a) without and (b) with DVB as crosslinker; (c) ellipsoids formed by swelling and phase separation in one-step emulsion polymerization; (d) doublets produced by separate steps of swelling and phase separation. All scale bars are 400 nm. (e) Schematic illustration of the morphological dependence of Fe_3O_4@PS composite microspheres on the feeding ratio of St to Fe_3O_4 and concentration of cross-Linker DVB. (f) Synthesis scheme for Fe_3O_4@SiO_2@PS composite colloids by seeded emulsion polymerization. The morphology of the final products is determined by (A) interfacial tension, (B) crosslinking, as well as (C) single and (D) separate steps of swelling and phase separation (images e and f are reprinted from ref. 111 and 112, respectively, with permission).

polymer shell using a combined technique of heterocoagulation and soap-free emulsion polymerization. 2,2′-Azobis[*N*-(2-carboxyethyl)-2-2-methylpropionamidine] (VA-057) has been used to control the colloidal stability of the magnetic cores during polymerization.[115]

Environment-responsive nanocomposites produce stimuli behavior when subjected to an external factor such as temperature, pH, light, electric field, and magnetic field. Specifically, pH-responsive nanocomposites have aroused widespread interest from the perspective of drug carrier applications. The pH-sensitive hollow poly(*N,N*-methylenebisacrylamide-*co*-methacrylic acid) microspheres with movable magnetic/silica (Fe_3O_4/SiO_2) cores have been synthesized by distillation precipitation copolymerization of *N,N*-methylenebisacrylamide and methacrylic acid (MAA) in the presence of Fe_3O_4/SiO_2/PMAA tri-layer microspheres as seeds in acetonitrile.[116] Lee has synthesized poly(NIPAAm-MAA)/Fe_3O_4 hollow latex particles in three steps. The key of this method is that heating melts the soft core without breaking the shell structure, and after the reaction with NH_4OH and (Fe^{2+}, Fe^{3+}) ions that attach to the –COOH groups of the MAA segments, *in situ* generation of Fe_3O_4 nanoparticles can be achieved and the poly(NIPAAm-MAA)/Fe_3O_4 magnetic composite with hollow latex particles are formed.[117] Epoxy group-functionalized MNPs with core-shell, dispersed, and asymmetric microstructures can be obtained by modified miniemulsion polymerization. The epoxy group density on the surface can be controlled by a further seed polymerization. Mechanistic studies indicate that the cross linking agent DVB contributes to the faster polymerization rate thus helping the latex to form the shell matrix in the early stage of the reaction as well as subsequent polymerization.[118]

4. Applications of multifunctional magnetic nanoparticles to biomedical diagnosis and treatment

4.1 Multimodal imaging

Magnetic resonance imaging which is based on computer-assisted imaging of relaxation signals of proton spins within the human internal organs excited by radiofrequency waves under the gradient magnetic field has become a useful diagnostic tool in medical science. It offers several advantages such as non-invasiveness, possibility to generate 3D images, and strong signals from soft tissues.[119] The relaxation improvement of MRI contrast agents consists of shortening the longitudinal relaxation time (T_1) and transverse relaxation time (T_2) of protons located nearby. Typically, gadolinium-diethylene triamine pentaacetic acid (Gd-DTPA) is used as the T_1 contrast agent with positive contrast whereas the super-paramagnetic nanoparticles are selected as the T_2 negative contrast agent. It results in darkening of the corresponding area in the T_2-weighted MR images.[120] Super-paramagnetic iron oxide in the form of maghemite Fe_2O_3 or magnetite Fe_3O_4, metal alloys (FeCo and FePt), and paramagnetic europium Eu and Mn-containing materials also serve as MRI contrast agents. Hyeon *et al.* have synthesized uniform-sized

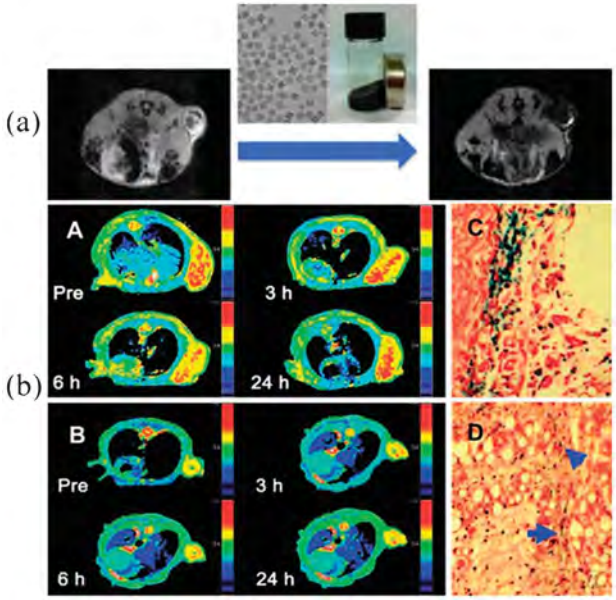

Fig. 8 (a) *In vivo* MR Images of the tumor site before and 1 h after intravenous injection of iron oxide nanocubes. After administration of iron oxide nanocubes, the MR signal of the tumor is significantly attenuated. (b) Animal MRI T_2 maps acquired before and after tail vein administration of Fa-$PEG_{4.3k}$-PCL_{1k}-SPION- (A) and $PEG_{4.3k}$-PCL_{1k}-SPION (B) into mice bearing a Bel 7402 tumor (about 0.5 cm in diameter) at a dose of 10 mg Fe kg^{-1} body weight. Prussian blue staining images (*200) of tumor sections excised from two mice after 3 h tail vein injection of Fa-$PEG_{4.3k}$-PCL_{1k}-PION (C) and $PEG_{4.3k}$-PCL_{1k}-SPION (D). The blue arrows in D indicate weak prussian blue stain (images a and b are reprinted from ref. 121 and 122, respectively, with permission).

iron oxide nanocubes with an edge length of 22 nm. They are encapsulated within the PEG-phospholipids and exhibit high colloidal stability in aqueous media. The theoretically predicted maximum of r_2 relativity is achieved by optimizing the overall size of ferrimagnetic iron oxide nanoparticles. The nanoparticles are injected intravenously into a nude mouse with melanoma for T_2-weighted MR imaging (Fig. 8a). Signal attenuation is clearly observed at the tumor site through an enhanced permeability and retention effect (EPR) due to the increased permeability of tumor endothelia and hypervasculature and lack of normal lymphatic drainage, demonstrating passive targeting imaging.[121] The biggest challenge of contrast agents is the behavior *in vivo*. MNPs are prone to forming aggregates. They absorb serum proteins during circulation and are mostly taken up by the RES (including the liver, spleen, and lymph nodes), thus affecting the effectiveness of diagnostic imaging. The targeted contrast agents accumulating around the target tissue are the key study issue and many attempts have been made to modify the surface of MNPs to add targeting ligands and achieve better control over agent pharmacokinetics. Cheng *et al.* have developed copolymers of poly(ethylene glycol) and poly(3-caprolactone) bearing folate as a targeting molecule (Fa-PEG-PCL) to encapsulate nonclustered super-paramagnetic iron oxide nanoparticle (SPION) to obtain water-dispersed and tumor-targeted MRI contrast agents. They simultaneously display increased transversal (r_2) and much decreased longitudinal (r_1) magnetic resonance

relaxivities as indicated by the large r_2/r_1 ratios. Injection of small-sized folate-targeted micelles (Fa-$PEG_{4.3k}$-PCL_{1k}-SPION) results in obviously shortened MRI T_2 as well as decreased MRI signal intensity in the tumor section (Fig. 8b), implying efficient accumulation of the micelles.[122]

Molecular imaging plays a very important role in medical treatment. Although some of the imaging modalities currently available can provide adequate images, most of them have inherent limitations such as low sensitivity as well as insufficient spatial or temporal resolution. Moreover, it is difficult to obtain all the necessary information about the biological structure and functions of an organ by a single imaging modality using existing imaging techniques.[123] Therefore, many attempts have been made to combine two or more imaging modalities while eliminating or reducing their disadvantages. These include the assessment of MRI/optical properties by MRI/PET, MRI/CT, and triple-modality imaging (Table 3).

4.1.1 MRI and optical imaging. Optical imaging is suitable for multimodal imaging due to its high sensitivity, spatial resolution in *in vitro* imaging, cost effectiveness, use of nonradioactive materials, and ability to provide cellular- or molecular-level information with almost single molecule sensitivity. However, the capability of obtaining anatomical and physiological details *in vivo* is relatively poor. In this respect, MRI provides comprehensive spatial resolution and excellently anatomic information, but unfortunately lacks the ability to image on the cellular level. Combination of MRI and optical imaging can improve the resolution and depth of imaging of the two modalities (MRI/optical properties). Techniques include MRI/Fluorescence,[125] MRI/NIR (near-infrared absorption),[126] and MRI/UCL (up-conversion luminescence phosphors).[127]

Organic fluorescent dyes like fluoresceinisothiocyanate and rhodamine, visible-fluorescent QDs, and sometimes molecules (*e.g.* carbazol) with fluorescence properties are commonly bounded to the surface of magnetic nanoparticles by covalent or other techniques to combine the magnetic and fluorescent properties. In particular, near-infrared absorption (700–1000 nm) has gained much attention due to the relatively low absorbance and scattering from living tissues in the NIR region of the spectrum. Organic fluorochromes (Cy5.5), nanosized semiconducor quantum dots, and gold can meet the requirements of NIR fluorophores. Near infrared-fluorescent QDs possess a number of significant optical properties, including a high quantum yield, broad absorption with narrow, symmetric photoluminescence spectra, high resistance to photobleaching, and chemical degradation. There are four different approaches to integrate the fluorescence and magnetic properties into one single nanoentity, namely growth of heterostructures, doping of paramagnetic ions into QDs, silica or polymer incorporation, and chelating molecules with paramagnetic ions on the shell of QDs.[128] Ma *et al.* have produced core/shell multilayered nanoprobes (MQQ nanoprobes) containing Fe_3O_4 nanoparticles, visible-fluorescent CdSe/ZnS QDs (600 nm emission), and near infrared-fluorescent CdSeTe/CdS QDs (780 nm emission) in multiple silica layers. The anti-HER2 (human epidermal growth factor receptor 2) antibody is conjugated to the surface of the MQQ nanoprobe for breast cancer tumor imaging. It is confirmed by fluorescence microscopy and fluorescence-activated cell sorting analysis *in vitro*. The *in vivo* multimodality images of breast tumors are acquired by NIR fluorescence and T_2-weighted magnetic resonance imaging.[129]

Organic fluorochromes typically exhibit rapid photobleaching and a low fluorescence quantum yield, whereas QDs are usually chemically unstable and potentially toxic and sometimes possess fluorescence intermittence. On the contrary, up-conversion luminescence phosphors show advantages of high-energy emission photons (visible wavelengths or near-infrared photon) in optical imaging after absorbing two or lower energy near-infrared photons in sequential adsorption and energy transfer steps. They can eliminate auto fluorescence from biological samples, minimize photo damage, and increase the penetration depth.[130] Lanthanide ions (Yb^{3+}, Er^{3+}, Tm^{3+} ions) have been incorporated into rare-earth fluoride compounds like $NaYF_4$ to yield visible emission upon IR excitation. Doping magnetic Gd^{3+} ions with the active contrast effect for MRI into the upconversion phosphor $NaYF_4$ host matrix generates biofunctional nanoparticles such as $NaYF_4$:Yb,Tm-$NaGdF_4$ core-shell nanoparticles,[131] $NaGdF_4$:Er^{3+},Yb^{3+}/$NaGdF_4$ core/shell up-converting nanoparticles,[132] and so on. The core-shell passive MRI contrast agents of Fe_3O_4@*n*SiO_2@*m*SiO_2@YVO_4:Eu^{3+},[133] and Fe_3O_4@SiO_2@Y_2O_3:Eu^{3+},[134] have magnetic and luminescent properties suitable for biomedical applications. The surface coating on the Fe_3O_4 core with silica or mesoporous silica can prevent the fluorescence from quenching by magnetite if

Table 3 Comparison of different imaging probe properties[124]

Modalities	Nanoprobes	Imaging properties
MRI	MNPs (*e.g.* Fe_3O_4, $MnFe_2O_4$) Metal alloy (*e.g.* FeCo, FePt) Paramagnetic nanoparticles (*e.g.* Gd_2O_3, MnO)	High spatial resolution, non-invasive, very good signal in soft-tissues
PET	Nanoparticles labeled with radionuclide (^{68}Ga, ^{18}F, ^{64}Cu, ^{76}Br, ^{86}Y, ^{89}Zr, ^{124}I)	High sensitivity which is an order of magnitude higher than that of MRI (picomolar level)
CT	Iodine, gold, and Bi_2S_3	High resolution, ease of forming 3D visual tissues, substantial doses of ionizing radiation
Optical imaging	Fluorescent organic dye (*e.g.* Cy5.5) visible-fluorescent QDs (*e.g.* near infrared, fluorescent), lanthanide atom (*e.g.* up-or down-conversion luminescence phosphors)	Rapid screening, cost effectiveness, poor anatomical and physiological details

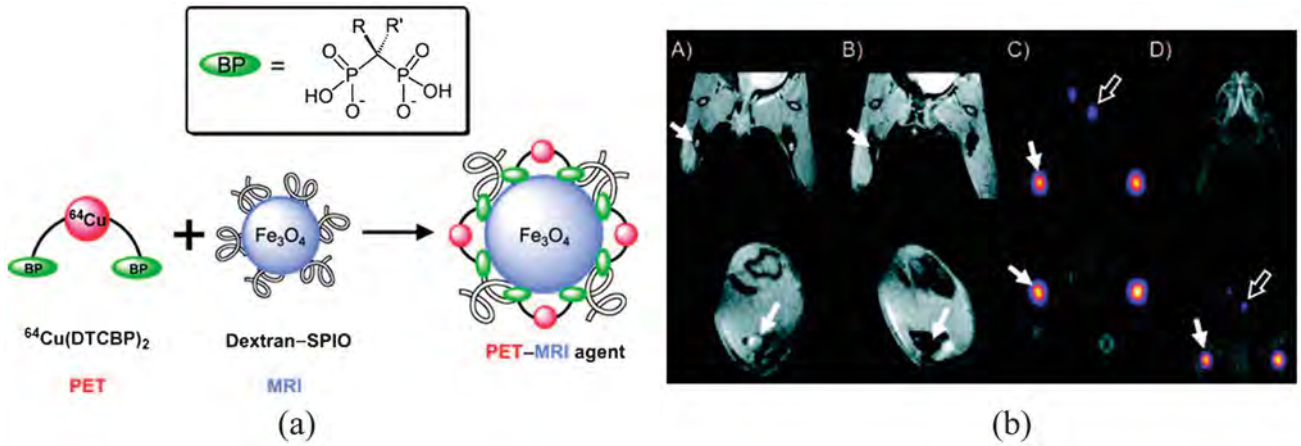

Fig. 9 (a) Schematic representation of the PET-MRI agent and (b) coronal (top) and short axis (bottom) MR images of the lower abdominal area and upper hind legs showing the popliteal lymph nodes (solid arrows) before (A) and after (B) footpad injection of [^{64}Cu(dtcbp)$_2$]–endorem. (C) Coronal (top) and short-axis (bottom) NanoPET-CT images and (D) whole-body nanoPET-CT images showing sole uptake of [^{64}Cu(dtcbp)$_2$]–endorem in the popliteal and iliac lymph nodes (images a and b are reprinted from ref. 140,with permission).

necessary. Yang *et al.* have developed monodispersed core-shell mesoporous Fe_3O_4@nSiO_2@mSiO_2@$NaYF_4$:Yb^{3+},Er^{3+}/Tm^{3+} with up-conversion luminescent and magnetic properties by a facile two-step sol–gel process.[135] The multifunctional composite is applied to the loading and controlled release of ibuprofen. The results show that it has unique properties including stable mesoporous structure, tunable pore size, high specific surface area, and easily modified surface boding well for applications to catalysis, bio-separation, and controlled drug release. Unique up-conversion emission (green for Yb^{3+}/Er^{3+} and blue for Yb^{3+}/Tm^{3+}) from the composites can be observed when excited by the 980 nm laser even after loading with drug molecules. The up-conversion emission intensity of the multifunctional carriers increases with the amount of released drug, thus allowing the drug release process to be monitored and tracked by changes in the photoluminescence intensity.

4.1.2 MRI and positron emission tomography (PET). Positron emission tomography (PET) is a sensitive human molecular imaging modality and produces whole body images with functional and molecular information, high sensitivity (picomolar level), and limitless tissue penetration. It also possesses the ability to detect and quantify exogenous radioactive isotopes accurately. Nanoparticles labeled with radionuclides such as ^{68}Ga, ^{18}F, ^{64}Cu, ^{76}Br, ^{86}Y, ^{89}Zr, and ^{124}I can be used in cardiovascular imaging, lung diagnosis, and tumor theranostics.[136] Meanwhile, magnetic resonance imaging (MRI) uses non-ionizing radiation and provides superior soft tissue contrast to CT. Combining PET with high-resolution MRI may lead to a breakthrough in the detection and monitoring of diseases. Chen *et al.* have reported nanoparticle-based probes in dual-modality PET/MRI by using MNPs as MRI agents and ^{124}I for PET.[137] Copper-based radionuclides that can offer a wide range of half-lives and positron energies are particularly interesting. Bao *et al.* have developed dual-modality nanoparticles for PET/MR imaging. They consist of a super-paramagnetic iron oxide (SPIO) core coated with PEGylated phospholipids, and chelator 1,4,7,10-tetraazacyclododecane-1,4,7,10-tetraacetic acid (DOTA) is conjugated to the PEG terminals to allow labeling with positron-emitting ^{64}Cu. Pharmacokinetics and the biodistribution of ^{64}Cu-mSPIO with stable and strong MR and PET signals reveal a circulation half-life of 143 min and high initial blood retention with moderate liver uptake. The results demonstrate the potential application as a dual-PET/MRI *in vivo* imaging probe.[138] Gong *et al.* have designed multifunctional MNPs nanocarriers for both tumor-targeted drug delivery and PET/MR imaging of tumors with integrin avb3 expression (Fig. 10). The anticancer drug DOX is conjugated to the PEGylated MNPs nanocarriers through pH-sensitive bonds, while cyclo(Arg-Gly-Asp-D-Phe-Cys) (c(RGDfC)) peptides and macrocyclic 1,4,7-triazacyclononane-*N,N,N*-triacetic acid (NOTA) are conjugated to the distal ends of the PEG arms. *In vitro* r_2 MRI relaxivity measurements confirm the effectiveness and the cRGD-conjugated MNPs nanocarriers also exhibit higher levels of tumor accumulation compared to cRGD-free SPIO nanocarriers according to *in vivo* PET imaging and biodistribution analyses.[139]

Except for chelates like DOTA with ^{64}Cu, Rosales *et al.* have described the design, synthesis, and characterization of dtcbp, a bifunctional chelator containing a dithiocarbamate group for binding of the PET isotope ^{64}Cu and bisphosphonate (bp) group to Fe_3O_4. The PET-MRI dual modality imaging capability of [^{64}Cu(dtcbp)$_2$]–endorem is demonstrated *in vivo* by accumulation in draining lymph nodes (Fig. 9). The *in vivo* uptake of [^{64}Cu(dtcbp)$_2$]–endorem can be easily and accurately quantified using the PET-MRI instrumentation.[140]

4.1.3 MRI and X-ray computed tomography (CT). X-Ray computed tomography (CT) probes based on iodine,[141] gold,[142] and Bi_2S_3[143] have many advantages due to the high resolution and ease of forming 3D visual tissues. Unlike the highly sensitive MRI, the inherently low sensitivity results in poor soft-tissue contrast and patients are typically exposed to substantial doses of ionizing radiation. Hence, the combination of MRI and CT is a hot research area. For instance,

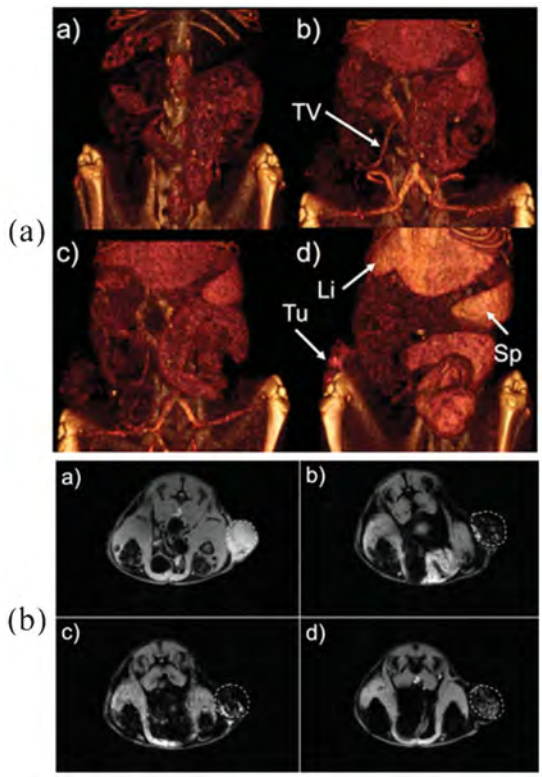

Fig. 10 (a) *In vivo* X-ray CT images of a rat: (a) before and (b) 1 h, (c) 2 h, and (d) 24 h after injection of Fe_3O_4/TaO_x (core/shell) MNPs (840 mg kg^{-1}). TV, Li, Tu, and Sp indicate the tumor-associated vessel, liver, tumor, and spleen, respectively. Fig. 9(b) *In vivo* T_2-weighted MRI images of a rat bearing a MAT III B tumor: (a) before and (b) 1 h, (c) 2 h, and (d) 24 h after the injection of Fe_3O_4/TaO_x (core/shell) MNPs (840 mg kg^{-1}) (emages a and b are reprinted from ref. 145, with permission).

functionalized gold nanoparticles (Au@DTDTPA-Gd) synthesized by reducing a gold salt ($HAuCl_4 \cdot 3H_2O$) with sodium borohydride ($NaBH_4$) in the presence of dithiolated derivatives of diethylenetriaminepenta acetic acid (DTDTPA) can be used as *in vivo* positive contrast agents in both MRI and X-ray imaging due to the high X-ray absorption coefficient of gold. In spite of the low gold (10 mg mL^{-1}) and gadolinium (5 mM) concentrations in the particles, they are easily detected and high sensitivity can be achieved.[144] Lee has reported the synthesis of multifunctional Fe_3O_4/TaO_x (core/shell) MNPs by the sol–gel reaction of tantalum(v) ethoxide in a microemulsion containing Fe_3O_4 nanoparticles (Fig. 10). They can provide complementary CT and MRI information. Therefore, newly formed tumors can be imaged by CT and the tumor microenvironment, including the hypoxic and oxygenated regions, can be evaluated by MRI. The core/shell MNPs have enormous potential in accurate cancer diagnosis by means of visualization of developed tumor vessels and monitoring of tumor status.[145]

4.1.4 Triple modality imaging. On the heels of the rapid development of biomedical imaging, triple-modality imaging probes in optical imaging/PET/MRI,[146] core-shell Fe_3O_4@$NaLuF_4$:Yb,Er/Tm nanostructure for MRI/CT/UCL imaging,[140] NaY/GdF_4:Yb, Er, Tm@SiO_2-Au@PEG_{5000} nanoprobes[147] for up conversion fluorescence/MR/CT imaging, and fluorine-18-labeled $Gd^{3+}/Yb^{3+}/Er^{3+}$co-doped $NaYF_4$ nanophosphors for PET/MR/UCL imaging[148] have attracted research interest. Li *et al.* have synthesized nanostructured core-shell Fe_3O_4@$NaLuF_4$:Yb,Er/Tm by a step-wise synthetic method. The Fe_3O_4 cores exhibit T_2-enhanced magnetic resonance (MR) effects with an r_2 value of 21.63 s^{-1} mM^{-1}, and computed tomography (CT) and UCL images confirm successful imaging of tumor-bearing mice utilizing the multifunctional nanocomposites.[149] Chen *et al.* have utilized dopamine to modify the surface of MNPs to yield nanoconjugates that can be easily encapsulated into human serum albumin (HSA) matrices (HSA-MNPs). To assess the biophysical characteristics of the nanoparticles, the HSA-MNPs are dually labeled with ^{64}Cu-DOTA and Cy5.5 and tested in a subcutaneous U87MG xenograft mouse model. *In vivo* positron emission tomography (PET)/near-infrared fluorescence (NIRF)/magnetic resonance imaging (MRI) tri-modality imaging and histological examination disclose that the particles have a good retention rate and high extravasation rate at the tumor sites (Fig. 11) and it is believed to stem from the HSA coating.[150]

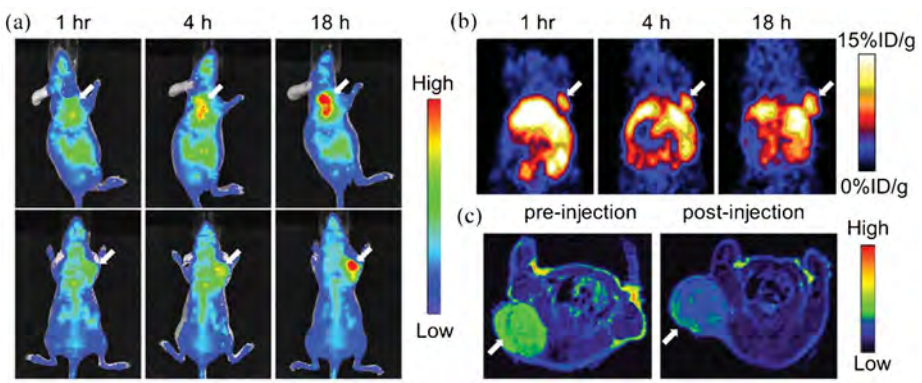

Fig. 11 (a) Representative *in vivo* NIRF images of mice injected with HSA-MNPs acquired 1 h, 4 h, and 18 h after injection. (b) *In vivo* PET imaging results of mice injected with HSA-MNPs acquired 1 h, 4 h, and 18 h after injection. (c) MRI images acquired before and 18 h after injection (reprinted from ref. 150, with permission).

4.2 Targeted drug and gene delivery

An interesting application of MNPs-based drug carriers is effective targeting to tumor sites by an external magnetic field where the drug is released locally. The side effect is prevented and the overall dose is reduced compared to traditional methods. In the early 1970s, Widder reported magnetic albumin microspheres loaded with doxorubicin for cancer treatment in rats. In recent years, more researchers have been studying magnetic nanoparticles as vehicles in drug delivery. The design of the drug delivery systems emphasizes delivery of DNA or RNA molecules,[151] targeting ligands (folic acid, peptides such as cyclic cRGD, transferrin and monoclonal antibodies), chemotherapeutics, as well as radioactive and hypothermic drugs. Generally, there are two methods to modify the MNPs, covalent conjugation and physical incorporation into the matrix like polymer or magnetic liposome. The process combines both the therapeutic and diagnostic elements in one entity. To achieve satisfactory therapeutic effects, the treatment conditions must be considered carefully.[152] For instance, the fate of the MNPs depends on multiple factors such as the temperature of the tissues, viscosity of the medium, external magnetic field gradient, fluid flow, size and size distributions, surface chemistry, and charge of the MNPs. It is believed that MNPs can be recognized as an invading agent by the reticuloendothelial system (RES system) and immediate absorption onto the surface may occur when unprotected MNPs are immersed in the blood stream. Hence, PEG with an optimal particle size from 10 to 100 nm is selected as the coating to evade the RES system and improve circulation time. The isoelectric point of MNPs should be around pH 7 which is similar to the physiological one. Liu *et al.* have fabricated organic/inorganic hybrid micelles using two amphiphilic block copolymers, poly(ε-caprolactone)-*b*-poly (glycerol monomethacrylate) (PCL-*b*-PGMA) and PCL-*b*-P (OEGMA-*co*-FA). The hydrophobic drugs are physically encapsulated in the micellar cores and super-paramagnetic iron oxide (SPIO) nanoparticles are embedded in the hydrophilic coronas. Controlled and sustained release of paclitaxel (PTX) demonstrates a ~61% cumulative release of the encapsulated drugs (loading content 8.5 w/w%) over 130 h and the clustering of SPIO nanoparticles in the micellar coronas can serve as the T_2-weighted MRI contrast agents with improved performance.[153] Meanwhile, magnetic drug targeting has been further extrapolated to deliver DNA/RNA to mammalian cells and tissues by adopting the physical principles of MNPs targeting. It has seen significant progress in recent years. Since Dobson first described MNPs-based gene transfection by linking viral vectors to magnetic carriers,[154] there has been extensive work on adapting this technique for non-viral transfection of biomolecules. Small interfering RNA (siRNA) with a short double-stranded RNA composed of 19–23 nucleotides is a potent therapeutic agent for numerous diseases because it can silence specific genes rapidly and efficiently. However, unlike conventional chemotherapeutics, the anionic and hydrophilic RNA molecules show rapid enzymatic degradation behavior in blood and cannot be internalized by cells by passive diffusion. To overcome these hurdles, various cationic polymers such as liposomes, cationic polymers, dendrimers, cell-penetrating peptides, semiconductor quantum dots, and magnetic nanoparticles have been utilized to produce compact polyelectrolyte complexes with siRNA.[155] For instance, Zhang *et al.* have developed a new multifunctional magnetic nanovector consisting of a super-paramagnetic iron oxide (Fe_3O_4) core coated with a cationic copolymer of chitosan-grafted-polyethelyne glycol (PEG) and cationic polyethylenimine (PEI). The product which is further functionalized with negatively-charged siRNA by electrostatic interaction shows improved efficacy in gene silencing through receptor mediated endocytosis. The targeting peptide chlorotoxin (CTX) is covalently attached to the nanoparticles to improve tumor specificity and to specifically knock down the transgene expression of green fluorescence protein (GFP) in C6/GFP glioma cells.[156]

4.3 Hyperthermia treatment for cancer

The possibility of treating cancer by artificially prompted hyperthermia has spurred the development of a variety of devices designed to heat tumor cells and they are promising in thermotherapy treatments. The purpose of hyperthermia is to deliberately heat tumor regions without damaging the healthy tissues and cells. The biomedical basis for hyperthermia treatment is that cancer cells are much more sensitive to temperature than normal tissues. MNPs have a high specific absorption rate (SAR) and hyperthermic effects occur in the range of 41 to 46 °C because of the altered structure and enzymatic functions of cell proteins. This is accompanied by cell carbonization at 50 °C.[157,158] The MNPs provides the heat by Brown relaxation due to the friction arising from total particle oscillations and Neel relaxation arising from the rotation of the magnetic moment with each field oscillation in an alternating magnetic field.[159] There have been reports describing magnetic nanoparticles as thermotherapy agents *in vitro* and *in vivo* for multiple types of cancer, including recurrent malignant astrocytic brain tumors, breast and prostate cancer, malignant melanoma, lymph node metastasis, glioblastoma, cervical carcinoma, and head and neck squamous cell carcinoma.[160–163] The outcome of the hyperthermia treatment depends on the following factors: particle size and distribution, magnetic susceptibility, accurate control of temperature, and heating and activation of the immune response.

In 2006, Jordan's group reported the tolerability and feasibility using MNPs in patients on recurrent glioblastoma multiforme. The study successfully demonstrates that thermotherapy using MNPs can be applied safely in treating brain tumors.[164] Johannsen has studied the feasibility of biocompatible MNPs in thermotherapy and demonstrated that the hyperthermic to thermoablative temperature can be achieved in the prostates at relatively low magnetic field strengths through interstitial heating. Sufficiently durable interstitial deposition and homogeneous distribution of MNPs in the prostates are used to evaluate the suitability of the CT-based approach in quality control.[165] Hyeon *et al.* have developed chitosan-DOPA-stabilized-ferrimagnetic iron oxide nanocubes as an effective heat nanomediator for cancer hyperthermia. They enable successful eradication of cancer cells through caspase-mediated apoptosis (Fig. 12). These nanocomposites

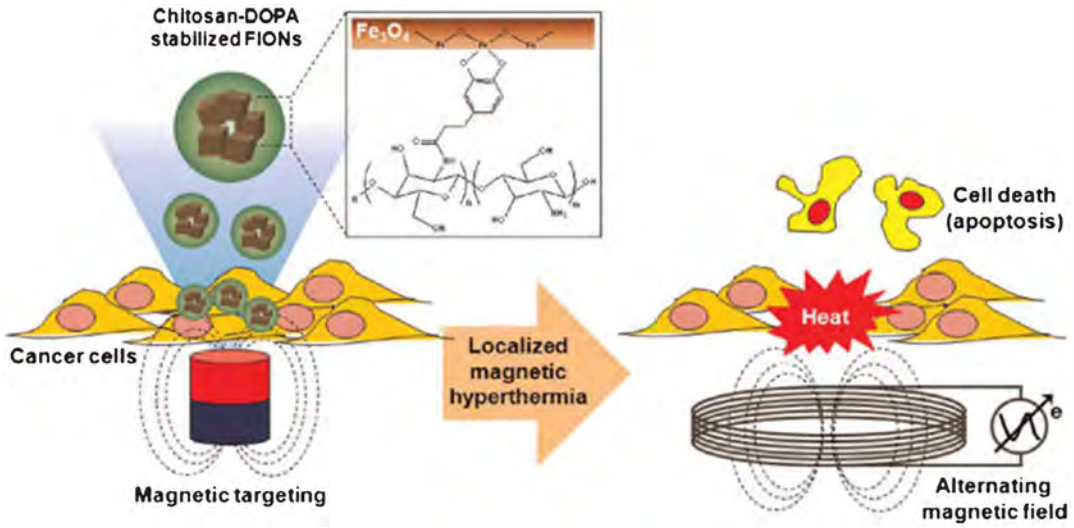

Fig. 12 Schematic illustration of the structure of chito-MNP and application to localized magnetic hyperthermia of cancer cells (reprinted from ref. 166, with permission).

also show excellent antitumor efficacy in an animal tumor model without showing severe toxicity.[166]

As a result of these encouraging results, targeted hyperthermia combining MNPs with monoclonal antibodies aimed to the tumor region has gained substantial attention. Tumor regression can be achieved and non-specific binding to healthy tissues can be overcome using the MNPs. As an alternative to radiotherapy and chemotherapy, significant progress has been made to targeted hyperthermia.[18] DeNardo confirms that ^{111}In-chimeric L6 (ChL6) monoclonal antibody (mAb)-linked iron oxide nanoparticles as immunoreactive bioprobes can be actively delivered to the tumors in athymic mice bearing the human breast cancer HBT 3477 xenografts and tumor regression is achieved at all alternating magnetic field levels.[167] Similarly, Rachakatla has used tumortropic neural progenitor cells in cell delivery vehicles for preferential accumulation of core/shell (iron/iron oxide) magnetic nanoparticles (MNPs) in mice bearing melanoma. All in all, tumor reduction after exposure to an alternating current magnetic field shows good potential as a cancer therapy modality with superior targeting.[168]

4.4 Other applications

Tremendous efforts have been made to use magnetic nanoparticles in cell therapies. In particular, magnetic nanoparticles coupled with mesenchymal stem cells can be directed to the desired sites for tissue repair. This is because stem cells can renew and produce other specialized cell types for transplantation purpose.[169] In addition, various types of cells such as erythrocytes and natural killer cells or proteins combined with magnetic nanoparticles can be delivered to the sites where they can play an important role in tissue repair.[170] In addition, nanoscale magnetic nanospheres can effectively remove and recover heavy ions from waste water by absorption and magnetic separation. The magnetic efficiency is determined by factors such as the size and surface area of the magnetic nanosphere, saturation magnetization, pH, temperature, as well as concentration of heavy ions and magnetic nanospheres.[171] Last but not least, magnetic nanoparticles can be used in biomedical separation, including separation of proteins, isolation of enzymes, and separation of nucleic acids and cells.[172,173]

5. Remarks and outlook

Multifunctional MNPs have received much attention due to their applications to the pharmaceutical and biomedical fields. There have been rapid developments in the synthesis and biomedical use of surface functionalized MNPs. New molecular probes have been developed to integrate optical imaging (fluorescent dyes, QDs, NIR, UCL) and positron emission tomography or X-ray computed tomography with MRI. Despite the tremendous potential, there are still considerable challenges, for example, controlled synthesis of MNPs with perfectly uniform magnetic loading and geometric shape. At present, they have only been used in MRI diagnosis and how to integrate with other imaging techniques to obtain more accurate and reliable medical information is still challenging. As therapeutic carriers, especially in gene therapy and targeted drug delivery, MNPs must be mobile in the body and so the distribution, biocompatibility, *in vivo* transport stability, and external magnetic field arrangement must still be improved. Last but not least, extensive applications of MNPs to chemotherapy and physical therapy still require extensive research but nonetheless, recent advances in the development of multifunctional magnetic nanoparticles and protocols suggest a bright future of MNPs in the diagnosis and therapy of diseases.

Acknowledgements

The authors kindly acknowledge the support of the National Natural Science Foundation of China (Grant No. 51273058) and Hong Kong Research Grants Council (RGC) General Research Funds (GRF) Nos. 112510 and 112212.

References

1 F. M. Kievit and M. Zhang, *Acc. Chem. Res.*, 2011, **44**, 853.
2 S. Laurent, D. Forge, M. Port, A. Roch, C. Robic, L. Vander Elst and R. N. Muller, *Chem. Rev.*, 2008, **108**, 2064.
3 A. H. Latham and M. E. Williams, *Acc. Chem. Res.*, 2008, **41**, 411.
4 J. Gao, H. Gu and B. Xu, *Acc. Chem. Res.*, 2009, **42**, 1097.
5 Y. Tai, L. Wang, G. Yan, J.-M. Gao, H. Yu and L. Zhang, *Polym. Int.*, 2011, **60**, 976.
6 X. Chen, L. Li, X. Sun, Y. Liu, B. Luo, C. Wang, Y. Bao, H. Xu and H. Peng, *Angew. Chem., Int. Ed.*, 2011, **50**, 5486.
7 R. Qiao, C. Yang and M. Gao, *J. Mater. Chem.*, 2009, **19**, 6274.
8 R. Hao, R. Xing, Z. Xu, Y. Hou, S. Gao and S. Sun, *Adv. Mater.*, 2010, **22**, 2729.
9 Q. A. Pankhurst, J. Connolly, S. K. Jones and J. Dobson, *J. Phys. D: Appl. Phys.*, 2003, **36**, R167.
10 M. A. Willard, L. K. Kurihara, E. E. Carpenter, S. Calvin and V. G. Harris, *Int. Mater. Rev.*, 2004, **49**, 125.
11 H. Yang, C. Zhang, X. Shi, H. Hu, X. Du, Y. Fang, Y. Ma, H. Wu and S. Yang, *Biomaterials*, 2010, **31**, 3667.
12 L. Frullano and T. J. Meade, *JBIC, J. Biol. Inorg. Chem.*, 2007, **12**, 939.
13 P. D. Schellinger, O. Jansen, J. B. Fiebach, W. Hacke and K. Sartor, *Stroke*, 1999, **30**, 765.
14 L. Bouffier, H. H. Yiu and M. J. Rosseinsky, *Langmuir*, 2011, **27**, 6185.
15 J. E. Lee, N. Lee, H. Kim, J. Kim, S. H. Choi, J. H. Kim, T. Kim, I. C. Song, S. P. Park, W. K. Moon and T. Hyeon, *J. Am. Chem. Soc.*, 2009, **132**, 552.
16 K. K. Turaga and L. K. Kvols, *Ca-Cancer J. Clin.*, 2011, **61**, 113.
17 C. C. Berry and A. S. G. Curtis, *J. Phys. D: Appl. Phys.*, 2003, **36**, 198.
18 P. Cherukuri, E. S. Glazer and S. A. Curley, *Adv. Drug Delivery Rev.*, 2010, **62**, 339.
19 N. Minc, C. Fütterer, K. D. Dorfman, A. Bancaud, C. Gosse, C. Goubault and J.-L. Viovy, *Anal. Chem.*, 2004, **76**, 3770.
20 H. Gu, K. Xu, C. Xu and B. Xu, *Chem. Commun.*, 2006, 941.
21 W. Wang, Y. Xu, D. I. C. Wang and Z. Li, *J. Am. Chem. Soc.*, 2009, **131**, 12892.
22 S. Miltenyi, W. Müller, W. Weichel and A. Radbruch, *Cytometry*, 1990, **11**, 231.
23 B. Polyak, I. Fishbein, M. Chorny, I. Alferiev, D. Williams, B. Yellen, G. Friedman and R. J. Levy, *Proc. Natl. Acad. Sci. U. S. A.*, 2008, **105**, 698.
24 D. M. Huang, J. K. Hsiao, Y. C. Chen, L. Y. Chien, M. Yao, Y. K. Chen, B. S. Ko, S. C. Hsu, L. A. Tai, H. Y. Cheng, S. W. Wang, C. S. Yang and Y. C. Chen, *Biomaterials*, 2009, **30**, 3645.
25 Y. Zhu, L. P. Stubbs, F. Ho, R. Liu, C. P. Ship, J. A. Maguire and N. S. Hosmane, *ChemCatChem*, 2010, **2**, 365.
26 N. Tran and T. J. Webster, *J. Mater. Chem.*, 2010, **20**, 8760.
27 M. Colombo, S. Carregal-Romero, M. F. Casula, L. Gutiérrez, M. P. Morales, I. B. Böhm, J. T. Heverhagen, D. Prosperi and W. J. Parak, *Chem. Soc. Rev.*, 2012, **41**, 4306.
28 L. H. Reddy, J. L. Arias, J. Nicolas and P. Couvreur, *Chem. Rev.*, 2012, **112**, 5818.
29 S. P. Massia, J. Stark and D. S. Letbetter, *Biomaterials*, 2000, **21**, 2253.
30 C. C. Berry, S. Wells, S. Charles and A. S. G. Curtis, *Biomaterials*, 2003, **24**, 4551.
31 J. K. Francis Suh and H. W. T. Matthew, *Biomaterials*, 2000, **21**, 2589.
32 A. Ito, M. Shinkai, H. Honda and T. Kobayashi, *J. Biosci. Bioeng.*, 2005, **100**, 1.
33 S. Bucak, D. A. Jones, P. E. Laibinis and T. A. Hatton, *Biotechnol. Prog.*, 2003, **19**, 477.
34 M. T. Peracchia, R. Gref, Y. Minamitake, A. Domb, N. Lotan and R. Langer, *J. Controlled Release*, 1997, **46**, 223.
35 R. Gref, A. Domb, P. Quellec, T. Blunk, R. H. Müller, J. M. Verbavatz and R. Langer, *Adv. Drug Delivery Rev.*, 1995, **16**, 215.
36 A. K. Gupta and S. Wells, *IEEE Trans. NanoBiosci.*, 2004, **3**, 66.
37 B. Xue and Y. Sun, *J. Chromatogr., A*, 2001, **921**, 109.
38 C. Brus, H. Petersen, A. Aigner, F. Czubayko and T. Kissel, *Bioconjugate Chem.*, 2004, **15**, 677.
39 J. D. Qiu, M. Xiong, R.-P. Liang, H.-P. Peng and F. Liu, *Biosens. Bioelectron.*, 2009, **24**, 2649.
40 J. L. Gong, Y. Liang, Y. Huang, J. W. Chen, J. H. Jiang, G. L. Shen and R. Q. Yu, *Biosens. Bioelectron.*, 2007, **22**, 1501.
41 D. K. Yi, S. T. Selvan, S. S. Lee, G. C. Papaefthymiou, D. Kundaliya and J. Y. Ying, *J. Am. Chem. Soc.*, 2005, **127**, 4990.
42 V. Georgakilas, V. Tzitzios, D. Gournis and D. Petridis, *Chem. Mater.*, 2005, **17**, 1613.
43 V. K. LaMer and R. H. Dinegar, *J. Am. Chem. Soc.*, 1950, **72**, 4847.
44 A. K. Gupta and M. Gupta, *Biomaterials*, 2005, **26**, 3995.
45 S. Mornet, S. Vasseur, F. Grasset and E. Duguet, *J. Mater. Chem.*, 2004, **14**, 2161.
46 R. Massart, *IEEE Trans. Magn.*, 1981, **323**, 133.
47 K. T. Wu, P. C. Kuo, Y. D. Yao and E. H. Tsai, *IEEE Trans. Magn.*, 2001, **37**, 2651.
48 C. Pereira, A. M. Pereira, C. Fernandes, M. Rocha, R. Mendes, M. P. Fernández-García, A. Guedes, P. B. Tavares, J.-M. Grenèche, J. P. Araújo and C. Freire, *Chem. Mater.*, 2012, **24**, 1496.
49 Y. Zhu, T. Mei, Y. Wang and Y. Qian, *J. Mater. Chem.*, 2011, **21**, 11457.
50 X. Sun, C. Zheng, F. Zhang, Y. Yang, G. Wu, A. Yu and N. Guan, *J. Phys. Chem. C*, 2009, **113**, 16002.
51 J. Ge, Y. Hu and Y. Yin, *Angew. Chem.*, 2007, **119**, 7572.
52 L. Wang, J. Bao, L. Wang, F. Zhang and Y. Li, *Chem.–Eur. J.*, 2006, **12**, 6341.
53 T. Hyeon, S. S. Lee, J. Park, Y. Chung and H. B. Na, *J. Am. Chem. Soc.*, 2001, **123**, 12798.
54 S. Sun and H. Zeng, *J. Am. Chem. Soc.*, 2002, **124**, 8204.

55 S. Sun, H. Zeng, D. B. Robinson, S. Raoux, P. M. Rice, S. X. Wang and G. Li, *J. Am. Chem. Soc.*, 2003, **126**, 273.
56 H. Kura, M. Takahashi and T. Ogawa, *J. Phys. Chem. C*, 2010, **114**, 5835.
57 E. V. Shevchenko, D. V. Talapin, A. L. Rogach, A. Kornowski, M. Haase and H. Weller, *J. Am. Chem. Soc.*, 2002, **124**, 11480.
58 S. Sun, *Adv. Mater.*, 2006, **18**, 393.
59 Z. Li, H. Chen, H. Bao and M. Gao, *Chem. Mater.*, 2004, **16**, 1391.
60 Z. Li, L. Wei, M. Y. Gao and H. Lei, *Adv. Mater.*, 2005, **17**, 1001.
61 Q. Jia, J. Zeng, R. Qiao, L. Jing, L. Peng, F. Gu and M. Gao, *J. Am. Chem. Soc.*, 2011, **133**, 19512.
62 Z. Xu, Y. Hou and S. Sun, *J. Am. Chem. Soc.*, 2007, **129**, 8698.
63 Y. Shi, H. Li, L. Wang, W. Shen and H. Chen, *ACS Appl. Mater. Interfaces*, 2012, **4**, 4800.
64 W. Wu, S. Zhang, X. Xiao, J. Zhou, F. Ren, L. Sun and C. Jiang, *ACS Appl. Mater. Interfaces*, 2012, **4**, 3602.
65 H. Yu, M. Chen, P. M. Rice, S. X. Wang, R. L. White and S. Sun, *Nano Lett.*, 2005, **5**, 379.
66 H. Zhang, X. Zhong, J.-J. Xu and H.-Y. Chen, *Langmuir*, 2008, **24**, 13748.
67 J. Gao, G. Liang, B. Zhang, Y. Kuang, X. Zhang and B. Xu, *J. Am. Chem. Soc.*, 2007, **129**, 1428.
68 H. Tüysüz, E. L. Salabaş, E. Bill, H. Bongard, B. Spliethoff, C. W. Lehmann and F. Schüth, *Chem. Mater.*, 2012, **24**, 2493.
69 J. Gao, G. Liang, J. S. Cheung, Y. Pan, Y. Kuang, F. Zhao, B. Zhang, X. Zhang, E. X. Wu and B. Xu, *J. Am. Chem. Soc.*, 2008, **130**, 11828.
70 F. Jiao, A. Harrison, J. C. Jumas, A. V. Chadwick, W. Kockelmann and P. G. Bruce, *J. Am. Chem. Soc.*, 2006, **128**, 5468.
71 Y. Tsujii, K. Ohno, S. Yamamoto, A. Goto and T. Fukuda, *Adv. Polym. Sci.*, 2006, **197**, 1.
72 K. Ohno, T. Akashi, Y. Huang and Y. Tsujii, *Macromolecules*, 2010, **43**, 8805.
73 R. Barbey, L. Lavanant, D. Paripovic, N. Schüwer, C. Sugnaux, S. Tugulu and H. A. Klok, *Chem. Rev.*, 2009, **109**, 5437.
74 Y. Wang, X. Teng, J. S. Wang and H. Yang, *Nano Lett.*, 2003, **3**, 789.
75 X. Lu, R. Jiang, Q. Fan, L. Zhang, H. Zhang, M. Yang, Y. Ma, L. Wang and W. Huang, *J. Mater. Chem.*, 2012, **22**, 6965.
76 C. Huang, K. G. Neoh and E.-T. Kang, *Langmuir*, 2012, **28**, 563.
77 A. P. Majewski, A. Schallon, V. Jérôme, R. Freitag, A. H. E. Müller and H. Schmalz, *Biomacromolecules*, 2012, **13**, 857.
78 J. Liu, W. He, L. Zhang, Z. Zhang, J. Zhu, L. Yuan, H. Chen, Z. Cheng and X. Zhu, *Langmuir*, 2011, **27**, 12684.
79 H. Wang, W. Luo and J. Chen, *J. Mater. Sci.*, 2012, **47**, 5918.
80 Q. Li, L. Zhang, L. Bai, Z. Zhang, J. Zhu, N. Zhou, Z. Cheng and X. Zhu, *Soft Matter*, 2011, **7**, 6958.
81 R. Matsuno, K. Yamamoto, H. Otsuka and A. Takahara, *Macromolecules*, 2004, **37**, 2203.
82 C. Wang, Z. Wang and X. Zhang, *Acc. Chem. Res.*, 2012, **45**, 608.
83 D. Niu, X. Liu, Y. Li, Z. Ma, W. Dong, S. Chang, W. Zhao, J. Gu, S. Zhang and J. Shi, *J. Mater. Chem.*, 2011, **21**, 13825.
84 G. Gao, H. Heo, J. Lee and D. Lee, *J. Mater. Chem.*, 2010, **20**, 5454.
85 H. Ai, C. Flask, B. Weinberg, X. T. Shuai, M. D. Pagel, D. Farrell, J. Duerk and J. Gao, *Adv. Mater.*, 2005, **17**, 1949.
86 B. S. Kim, J.-M. Qiu, J.-P. Wang and T. A. Taton, *Nano Lett.*, 2005, **5**, 1987.
87 R. J. Hickey, A. S. Haynes, J. M. Kikkawa and S.-J. Park, *J. Am. Chem. Soc.*, 2011, **133**, 1517.
88 E. K. Lim, J. Yang, C. P. N. Dinney, J.-S. Suh, Y.-M. Huh and S. Haam, *Biomaterials*, 2010, **31**, 9310.
89 X. Li, H. Li, G. Liu, Z. Deng, S. Wu, P. Li, Z. Xu, H. Xu and P. K. Chu, *Biomaterials*, 2012, **33**, 3013.
90 L. E. Euliss, S. G. Grancharov, S. O'Brien, T. J. Deming, G. D. Stucky, C. B. Murray and G. A. Held, *Nano Lett.*, 2003, **3**, 1489.
91 J. F. Berret, N. Schonbeck, F. Gazeau, D. El Kharrat, O. Sandre, A. Vacher and M. Airiau, *J. Am. Chem. Soc.*, 2006, **128**, 1755.
92 S. Manju and K. Sreenivasan, *Langmuir*, 2011, **27**, 14489.
93 M. Yoon, Y. Kim and J. Cho, *ACS Nano*, 2011, **5**, 5417–5426.
94 J. Kim, J. E. Lee, S. H. Lee, J. H. Yu, J. H. Lee, T. G. Park and T. Hyeon, *Adv. Mater.*, 2008, **20**, 478.
95 F. Hu, K. G. Neoh and E.-T. Kang, *Macromol. Rapid Commun.*, 2009, **30**, 609.
96 R. G. Pearson and J. Songstad, *J. Am. Chem. Soc.*, 1967, **89**, 1827.
97 R. Hong, N. O. Fischer, T. Emrick and V. M. Rotello, *Chem. Mater.*, 2005, **17**, 4617.
98 Y. M. Huh, Y. W. Jun, H.-T. Song, S. Kim, J. S. Choi, J. H. Lee, S. Yoon, K. S. Kim, J. S. Shin, J. S. Suh and J. Cheon, *J. Am. Chem. Soc.*, 2005, **127**, 12387.
99 Y. W. Jun, Y. M. Huh, J. S. Choi, J. H. Lee, H. T. Song, S. KimKim, K. S. Yoon, J. S. Kim, J. S. Shin Suh and J. Cheon, *J. Am. Chem. Soc.*, 2005, **127**, 5732.
100 M. Kim, Y. Chen, Y. Liu and X. Peng, *Adv. Mater.*, 2005, **17**, 1429.
101 A. Hofmann, S. Thierbach, A. Semisch, A. Hartwig, M. Taupitz, E. Rühl and C. Graf, *J. Mater. Chem.*, 2010, **20**, 7842.
102 G. Huang, C. Zhang, S. Li, C. Khemtong, S. G. Yang, R. Tian, J. D. Minna, K. C. Brown and J. Gao, *J. Mater. Chem.*, 2009, **19**, 6367.
103 C. Xu, K. Xu, H. Gu, R. Zheng, H. Liu, X. Zhang, Z. Guo and B. Xu, *J. Am. Chem. Soc.*, 2004, **126**, 9938.
104 E. Amstad, S. Zurcher, A. Mashaghi, J. Y. Wong, M. Textor and E. Reimhult, *Small*, 2009, **5**, 1334.
105 E. Amstad, T. Gillich, I. Bilecka, M. Textor and E. Reimhult, *Nano Lett.*, 2009, **9**, 4042.
106 H. Lee, E. Lee, D. K. Kim, N. K. Jang, Y. Y. Jeong and S. Jon, *J. Am. Chem. Soc.*, 2006, **128**, 7383.
107 E. K. U. Larsen, T. Nielsen, T. Wittenborn, H. Birkedal, T. Vorup-Jensen, M. H. Jakobsen, L. Østergaard, M. R. Horsman, F. Besenbacher, K. A. Howard and J. Kjems, *ACS Nano*, 2009, **3**, 1947.

108 R. De Palma, S. Peeters, M. J. Van Bael, H. Van den Rul, K. Bonroy, W. Laureyn, J. Mullens, G. Borghs and G. Maes, *Chem. Mater.*, 2007, **19**, 1821.

109 N. Pothayee, N. Pothayee, N. Jain, N. Hu, S. Balasubramaniam, L. M. Johnson, R. M. Davis, N. Sriranganathan and J. S. Riffle, *Chem. Mater.*, 2012, **24**, 2056.

110 H. Kawaguchi, *Prog. Polym. Sci.*, 2000, **25**, 1171.

111 S. Xu, W. F. Ma, L. J. You, J. M. Li, J. Guo, J. J. Hu and C. C. Wang, *Langmuir*, 2012, **28**, 3271.

112 J. Ge, Y. Hu, T. Zhang and Y. Yin, *J. Am. Chem. Soc.*, 2007, **129**, 8974.

113 H. Liu, C. Wang, Q. Gao, X. Liu and Z. Tong, *Acta Biomater.*, 2010, **6**, 275.

114 C. Okoli, M. Sanchez-Dominguez, M. Boutonnet, S. Järås, C. Civera, C. Solans and G. R. Kuttuva, *Langmuir*, 2012, **28**, 8479.

115 D. Nagao, M. Yokoyama, N. Yamauchi, H. Matsumoto, Y. Kobayashi and M. Konno, *Langmuir*, 2008, **24**, 9804.

116 G. Liu, H. Wang and X. Yang, *Polymer*, 2009, **50**, 2578.

117 C. F. Lee, M. L. Lin, Y. C. Wang and W. Y. Chiu, *J. Polym. Sci., Part A: Polym. Chem.*, 2012, **50**, 2626.

118 Y. Xu, H. Xu and H. Gu, *J. Polym. Sci., Part A: Polym. Chem.*, 2010, **48**, 2284.

119 H. B. Na, I. C. Song and T. Hyeon, *Adv. Mater.*, 2009, **21**, 2133.

120 B. H. Kim, N. Lee, H. Kim, K. An, Y. I. Park, Y. Choi, K. Shin, Y. Lee, S. G. Kwon, H. B. Na, J.-G. Park, T.-Y. Ahn, Y.-W. Kim, W. K. Moon, S. H. Choi and T. Hyeon, *J. Am. Chem. Soc.*, 2011, **133**, 12624.

121 N. Lee, Y. Choi, Y. Lee, M. Park, W. K. Moon, S. H. Choi and T. Hyeon, *Nano Lett.*, 2012, **12**, 3127.

122 D. Cheng, G. Hong, W. Wang, R. Yuan, H. Ai, J. Shen, B. Liang, J. Gao and X. Shuai, *J. Mater. Chem.*, 2011, **21**, 4796.

123 J. Kim, Y. Piao and T. Hyeon, *Chem. Soc. Rev.*, 2009, **38**, 372.

124 A. Louie, *Chem. Rev.*, 2010, **110**, 3146.

125 C. Wang and J. Irudayaraj, *Small*, 2010, **6**, 283.

126 Z. Xu, C. Li, X. Kang, D. Yang, P. Yang, Z. Hou and J. Lin, *J. Phys. Chem. C*, 2010, **114**, 16343.

127 Z. Chen, W. Bu, N. Zhang and J. Shi, *J. Phys. Chem. C*, 2008, **112**, 4378.

128 R. Koole, W. J. M. Mulder, M. M. van Schooneveld, G. J. Strijkers, A. Meijerink and K. Nicolay, *Wiley Interdiscip. Rev.: Nanomed. Nanobiotechnol.*, 2009, **1**, 475.

129 Q. Ma, Y. Nakane, Y. Mori, M. Hasegawa, Y. Yoshioka, T. M. Watanabe, K. Gonda, N. Ohuchi and T. Jin, *Biomaterials*, 2012, **33**, 8486.

130 Y. Cui, Y. Yue, G. Qian and B. Chen, *Chem. Rev.*, 2012, **112**, 1126.

131 C. Dong, A. Korinek, B. Blasiak, B. Tomanek and F. C. J. M. van Veggel, *Chem. Mater.*, 2012, **24**, 1297.

132 Y. I. Park, J. H. Kim, K. T. Lee, K. S. Jeon, H. B. Na, J. H. Yu, H. M. Kim, N. Lee, S. H. Choi, S. I. Baik, H. Kim, S. P. Park, B. J. Park, Y. W. Kim, S. H. Lee, S. Y. Yoon, I. C. Song, W. K. Moon, Y. D. Suh and T. Hyeon, *Adv. Mater.*, 2009, **21**, 4467.

133 P. Yang, Z. Quan, Z. Hou, C. Li, X. Kang, Z. Cheng and J. Lin, *Biomaterials*, 2009, **30**, 4786.

134 L. Tong, J. Shi, D. Liu, Q. Li, X. Ren and H. Yang, *J. Phys. Chem. C*, 2012, **116**, 7153.

135 S. Gai, P. Yang, C. Li, W. Wang, Y. Dai, N. Niu and J. Lin, *Adv. Funct. Mater.*, 2010, **20**, 1166.

136 Y. Liu and M. J. Welch, *Bioconjugate Chem.*, 2012, **23**, 671.

137 J. S. Choi, J. C. Park, H. Nah, S. Woo, J. Oh, K. M. Kim, G. J. Cheon, Y. Chang, J. Yoo and J. Cheon, *Angew. Chem., Int. Ed.*, 2008, **47**, 6259.

138 C. Glaus, R. Rossin, M. J. Welch and G. Bao, *Bioconjugate Chem.*, 2010, **21**, 715.

139 X. Yang, H. Hong, J. J. Grailer, I. J. Rowland, A. Javadi, S. A. Hurley, Y. Xiao, Y. Yang, Y. Zhang, R. J. Nickles, W. Cai, D. A. Steeber and S. Gong, *Biomaterials*, 2011, **32**, 4151.

140 R. Torres Martin de Rosales, R. Tavaré, R. L. Paul, M. Jauregui-Osoro, A. Protti, A. Glaria, G. Varma, I. Szanda and P. J. Blower, *Angew. Chem., Int. Ed.*, 2011, **50**, 5509.

141 Y. Liu, K. Ai and L. Lu, *Acc. Chem. Res.*, 2012, **45**, 1817.

142 I. C. Sun, D. K. Eun, H. Koo, C. Y. Ko, H. S. Kim, D. K. Yi, K. Choi, I. C. Kwon, K. Kim and C. H. Ahn, *Angew. Chem., Int. Ed.*, 2011, **50**, 9348.

143 O. Rabin, J. Manuel Perez, J. Grimm, G. Wojtkiewicz and R. Weissleder, *Nat. Mater.*, 2006, **5**, 118.

144 C. Alric, J. Taleb, G. L. Duc, C. Mandon, C. Billotey, A. L. Meur-Herland, T. Brochard, F. Vocanson, M. Janier, P. Perriat, S. Roux and O. Tillement, *J. Am. Chem. Soc.*, 2008, **130**, 5908.

145 N. Lee, H. R. Cho, M. H. Oh, S. H. Lee, K. Kim, B. H. Kim, K. Shin, T. Y. Ahn, J. W. Choi, Y. W. Kim, S. H. Choi and T. Hyeon, *J. Am. Chem. Soc.*, 2012, **134**, 10309.

146 J. C. Park, M. K. Yu, G. I. An, S.-I. Park, J. Oh, H. J. Kim, J.-H. Kim, E. K. Wang, I. H. Hong, Y. S. Ha, T. H. Choi, K.-S. Jeong, Y. Chang, M. J. Welch, S. Jon and J. Yoo, *Small*, 2010, **6**, 2863.

147 X. Zhu, J. Zhou, M. Chen, M. Shi, W. Feng and F. Li, *Biomaterials*, 2012, **33**, 4618.

148 H. Xing, W. Bu, S. Zhang, X. Zheng, M. Li, F. Chen, Q. He, L. Zhou, W. Peng, Y. Hua and J. Shi, *Biomaterials*, 2012, **33**, 1079.

149 J. Zhou, M. Yu, Y. Sun, X. Zhang, X. Zhu, Z. Wu, D. Wu and F. Li, *Biomaterials*, 2011, **32**, 1148.

150 J. Xie, K. Chen, J. Huang, S. Lee, J. Wang, J. Gao, X. Li and X. Chen, *Biomaterials*, 2010, **31**, 3016.

151 O. Veiseh, J. W. Gunn and M. Zhang, *Adv. Drug Delivery Rev.*, 2010, **62**, 284.

152 P. M. Valencia, P. A. Basto, L. Zhang, M. Rhee, R. Langer, O. C. Farokhzad and R. Karnik, *ACS Nano*, 2010, **4**, 1671.

153 J. Hu, Y. Qian, X. Wang, T. Liu and S. Liu, *Langmuir*, 2012, **28**, 2073.

154 J. Dobson, *Drug Dev. Res.*, 2006, **67**, 55.

155 K. H. Bae, K. Lee, C. Kim and T. G. Park, *Biomaterials*, 2011, **32**, 176.

156 O. Veiseh, F. M. Kievit, C. Fang, N. Mu, S. Jana, M. C. Leung, H. Mok, R. G. Ellenbogen, J. O. Park and M. Zhang, *Biomaterials*, 2010, **31**, 8032.

157 Q. A. Pankhurst, N. T. K. Thanh, S. K. Jones and J. Dobson, *J. Phys. D: Appl. Phys.*, 2009, **42**, 224001.

158 A. K. Gupta, R. R. Naregalkar, V. D. Vaidya and M. Gupta, *Nanomedicine*, 2007, **2**, 73.

159 J. P. Fortin, F. Gazeau and C. Wilhelm, *Eur. Biophys. J.*, 2007, **37**, 223.

160 Y. Arum, Y. Song and J. Oh, *Appl. Nanosci.*, 2011, **1**, 237.
161 M. Shinkai, *J. Biosci. Bioeng.*, 2002, **94**, 606.
162 K. Maier-Hauff, F. Ulrich, D. Nestler, H. Niehoff, P. Wust, B. Thiesen, H. Orawa, V. Budach and A. Jordan, *J. Neuro-Oncol.*, 2010, **103**, 317.
163 W. Walther, F. Arlt, I. Fichtner, J. Aumann, U. Stein and P. M. Schlag, *Mol. Cancer Ther.*, 2007, **6**, 236.
164 K. Maier Hauff, R. Rothe, R. Scholz, U. Gneveckow, P. Wust, B. Thiesen, A. Feussner, A. Deimling, N. Waldoefner, R. Felix and A. Jordan, *J. Neuro-Oncol.*, 2006, **81**, 53.
165 M. Johannsen, U. Gneveckow, B. Thiesen, K. Taymoorian, C. H. Cho, N. Waldöfner, R. Scholz, A. Jordan, S. A. Loening and P. Wust, *Eur. Urol.*, 2007, **52**, 1653.
166 K. H. Bae, M. Park, M. J. Do, N. Lee, J. H. Ryu, G. W. Kim, C. Kim, T. G. Park and T. Hyeon, *ACS Nano*, 2012, **6**, 5266.
167 S. J. DeNardo, *Clin. Cancer Res.*, 2005, **11**, 7087.
168 R. S. Rachakatla, S. Balivada, G.-M. Seo, C. B. Myers, H. Wang, T. N. Samarakoon, R. Dani, M. Pyle, F. O. Kroh, B. Walker, X. Leaym, O. B. Koper, V. Chikan, S. H. Bossmann, M. Tamura and D. L. Troyer, *ACS Nano*, 2010, **4**, 7093.
169 M. Modo, D. Cash, K. Mellodew, S. C. R. Williams, S. E. Fraser, T. J. Meade, J. Price and H. Hodges, *NeuroImage*, 2002, **17**, 803.
170 C. W. Lu, Y. Hung, J.-K. Hsiao, M. Yao, T.-H. Chung, Y.-S. Lin, S.-H. Wu, S. C. Hsu, H. M. Liu, C. Y. Mou, C. S. Yang, D. M. Huang and Y.-C. Chen, *Nano Lett.*, 2006, **7**, 149.
171 M. Takafuji, S. Ide, H. Ihara and Z. Xu, *Chem. Mater.*, 2004, **16**, 1977.
172 I. S. Lee, N. Lee, J. Park, B. H. Kim, Y.-W. Yi, T. Kim, T. K. Kim, I. H. Lee, S. R. Paik and T. Hyeon, *J. Am. Chem. Soc.*, 2006, **128**, 10658.
173 T. Neuberger, B. Schöpf, H. Hofmann, M. Hofmann and B. von Rechenberg, *J. Magn. Magn. Mater.*, 2005, **293**, 483.

